Charles University in Prague Faculty of Mathematics and Physics

RIGOROUS THESIS

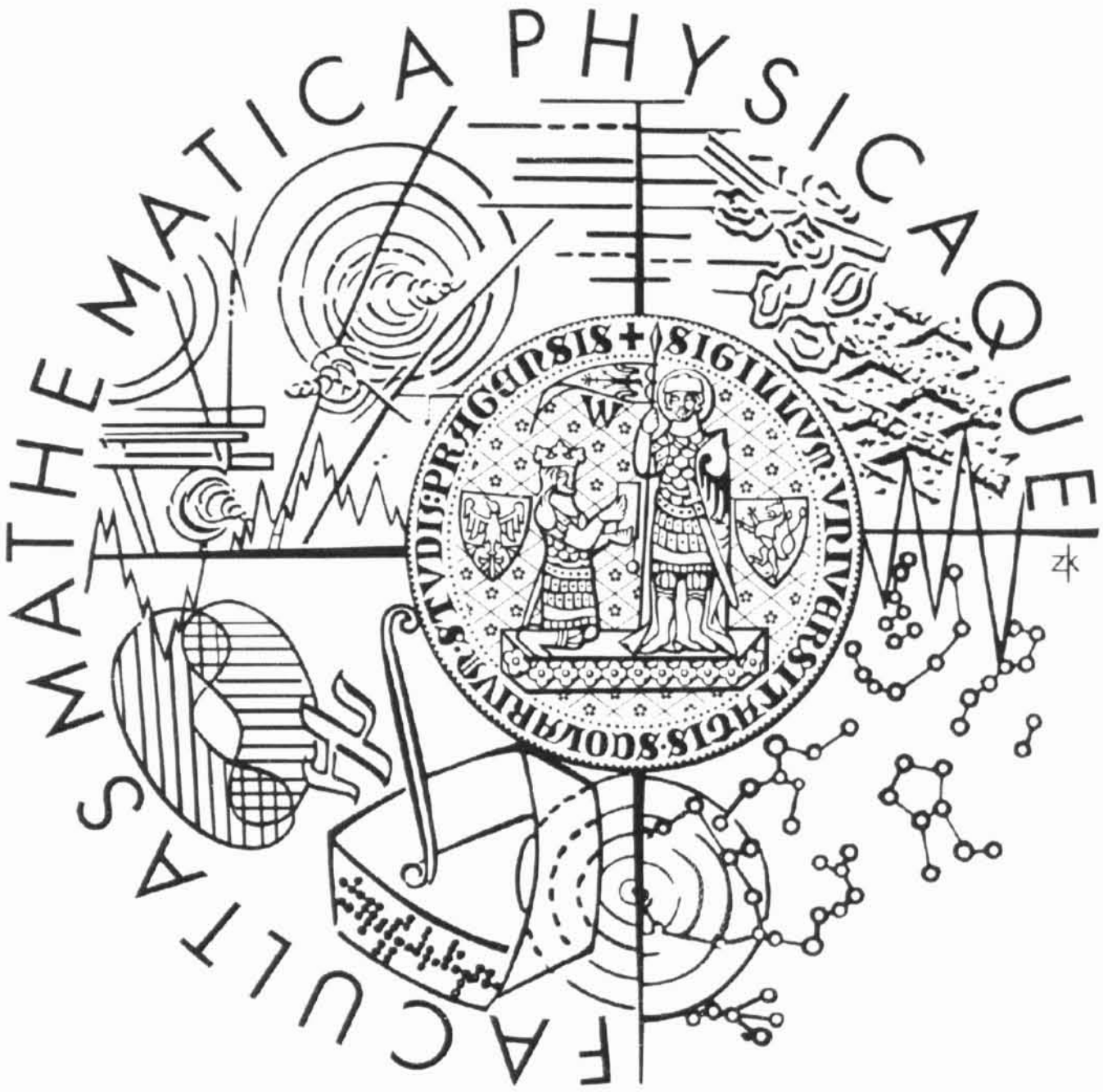

Petr Kovář

Molecular modeling of layered double hydroxides intercalated with small organic anions

Department of Chemical Physics and Optics
Rigorous Thesis Supervisor: RNDr. Miroslav Pospíšil, Ph.D.
Study Field: Biophysics, Chemical and Macromolecular Physics

I thank very much for discussions, advise and help from my supervisor

RNDr. Miroslav Pospíšil, Ph.D.

Hereby I confirm that I wrote this thesis entirely by myself and with the use of listed references. I agree with lending this thesis.

Prague, May 9th 2008 Petr Kovář

Contents

Title: Molecular modeling of layered double hydroxides intercalated with small organic anions
Author: *Petr Kovář*
Department: *Department of Chemical Physics and Optics*
Supervisor: *RNDr. Miroslav Pospíšil, Ph.D.*
Supervisor's e-mail address: pospisil@karlov.mff.cuni.cz

Abstract:
The samples of Zn_4-Al_2 and Mg_4-Al_2 layered double hydroxides (LDHs) intercalated with benzoate anions and its derivatives (p-methylbenzoate and p-bromobenzoate) were prepared and characterized by powder X-ray diffraction, chemical analysis and thermogravimetry. The interlayer arrangement was calculated by molecular modeling combined with X-ray diffraction. Molecular mechanics and classical molecular dynamics were carried out in *Cerius*^{2} modeling environment. In the case of LDH intercalated with benzoate the guests adopt as the best a parquet arrangement in the interlayer space. The addition of CH_3 groups and Br atoms in the p-positions of the benzoate ring causes a disorientation of the guests. The interlayer water molecules are located in the planes with COO^- groups near the LDH layers. The strategy leading to solving of interlayer arrangement of LDH (LDH layers were kept as rigid units during the energy minimization and NVT statistical ensemble was used during the dynamics simulations) was successfully applicated in the case of LDH intercalated with bulky anions (porphyrin derivatives anions).

Keywords: layered double hydroxides, powder X-ray diffraction, molecular modeling

Název práce: Molekulární modelování podvojných vrstevnatých hydroxidů interkalovaných malými organickými anionty
Autor: Petr Kovář
Katedra (ústav): *Katedra chemické fyziky a optiky*
Vedoucí diplomové práce: *RNDr. Miroslav Pospíšil, Ph.D.*
e-mail vedoucího: pospisil@karlov.mff.cuni.cz

Abstrakt:
Byly připraveny vzorky podvojného vrstevnatého hydroxidu (LDH) typu Zn_4-Al_2 a Mg_4-Al_2 interkalovaného benzoátovými anionty a jejich deriváty (p-methylbenzoátem a p-bromobenzoátem). Vzorky byly charakterizovány pomocí práškové rentgenové difrakce, chemické analýzy a termogravimetrie. Uspořádání mezivrství bylo zkoumáno metodou kombinace molekulárního modelování a práškové difrakce. Molekulární mechanika a klasická molekulární dynamika byly provedeny v programu *Cerius*^{2}. V případě LDH interkalovaného benzoátem hosté zaujímají v mezivrstevném prostoru parketové uspořádání. Výskytem skupin CH_3 a atomů bromu v para pozicích benzenového jádra dojde k neuspořádání hostů v mezivrstevném prostoru. Mezivrstevná voda se nachází v rovinách spolu s karboxylovými skupinami podél LDH vrstev. Strategie vedoucí k vyřešení mezivrstevného uspořádání (vrstvy LDH drženy jako rigidní jednotky v průběhu minimalizace energie a užití NVT statistického souboru při molekulární dynamice) byla úspěšně aplikována v případě LDH interkalovaného velkými anionty (anionty derivátů porfyrinu).

Klíčová slova: podvojné vrstevnaté hydroxidy, prášková rentgenová difrakce, molekulární modelování

1. Introduction

1.1 Motivation and the aim of the work

The methods of structure analysis based on combination of molecular modeling and experiments help us to describe disordered, usually powder structures in details that cannot be analyzed by diffraction methods only. Chemical and physical properties of the materials strongly depend on the structure and molecular modeling is able to help us to describe the structure-properties relationship. Generally, the intercalation of various species into layered structures is very attractive because of a possibility of designing new materials with desirable properties [1, 2, 3]. Suitable compounds for the intercalation of organics or inorganic species are clay minerals; especially in this work Layered Double Hydroxides (LDHs). The intercalation of LDH can be based on ion-exchange reactions. One unique property of these solids is that after a thermal decomposition under mild conditions, they are able to recover the layered structure. It makes them different from cationic clays. This property represents a synthetic route for analogues of LDH and for the new intercalates [4, 5]. The LDH offer a large scale of possibilities and applications of these materials which are widening very fast. In the last twenty years, as a result of the advent of powerful affordable personal computers together with interactive, high resolution computer graphics terminals and the development of very sophisticated multifunctional software packages, molecular modeling has found a widespread usage in different research areas and one is also able to carry out simulations of large systems where ab-initio calculations would be still too time consuming.

In the present work we focused on the solving of the Zn_4-Al_2 LDH structure intercalated with benzoate anions and Mg_4-Al_2 LDH intercalated with p-methylbenzoate and p-bromobenzoate. The systems containing benzoate anions and benzoate derivatives were widely studied from experimental point of view [6-14]. The present structure analysis is based on the combination of molecular modeling, X-ray diffraction spectroscopy and thermogravimetry. The aims of the present work are:

1/ to work out methods of structure analysis and strategies of modeling of these small structures based on X-ray diffraction that would be subsequently applicable for bigger systems containing thousands of atoms (for example LDH + porphyrin derivatives intercalates)

2/ to determine the structure of Zn_4-Al_2 LDH intercalated with benzoate anions and the structure of Mg_4-Al_2 LDH intercalated with p-methylbenzoate and p-bromobenzoate anions.

2. Layered Double Hydroxides

The term of Layered Double Hydroxide is used to designate synthetic or natural lamellar hydroxides with two kinds of metallic cations in the main layers and interlayer domains containing anionic species. This wide family of compounds is also referred to as *anionic clays*, by comparison with the more usual cationic clays whose interlamellar domains contain cationic species [15]. LDHs are also reported as hydrotalcite-like compounds by reference to one of the polytypes of the corresponding Mg-Al based mineral. More seldom, they are named pyroaurite-like compounds, lamellar hydroxides of transition metals or mixed metallic hydroxides. The first natural mineral belonging to this family was discovered in Sweden in the 1842 and it is known as hydrotalcite. Its formula was $Mg_6Al_2\ (OH)_{16}\ CO_3 * 4H_2O$. The first studies on the synthesis, stability, solubility and structure determination are dated in 1930s. The structure of the layers of LDH is based on $M(OH)_6$ octahedral units sharing their edges in order to build $M(OH)_2$ brucite-like layers. These octahedral units contain both divalent (M^{II}) and trivalent (M^{III}) metallic cations; the LDH layers are therefore positively charged, and the charge density is proportional to the trivalent metal ratio:

$$x = \frac{M^{III}}{M^{II} + M^{III}}. \qquad (2.1)$$

The whole structure of LDH is consisted by stacking of such layers, and between the layers, there are intercalating charge-balancing anionic species and water molecules as it is shown in the figure 2.1. The general formula for LDH is

$$\left[M^{II}_{1-x}\ M^{III}_{x}\ (OH)_2\right]^{x+}\ \left[X^{m-}_{x/m}.nH_2O\right]^{x-}, \qquad (2.2)$$

where X is an exchangeable anion, n represents number of water molecules and m is a valence of interlayer anion.

Most of LDH systems accommodate a relatively wide range of trivalent ratios, but it is not reported that it could vary from 0 to 1 without main structural changes. The trivalent ratio lies between the x values of 0.2 and 0.4. The upper limit of trivalent ratio is generally attributed to electrostatic repulsion between trivalent metals in the layers and to repulsion between the charge-balancing anionic interlamellar species. The lower limit corresponds to lower electrostatic interactions between the layers and the interlamellar anions leading to a collapse of the interlamellar domains.

The divalent and trivalent metal cations found in LDHs belong mainly to the third and the fourth periods of the periodic table of the elements:

divalent cations: Mg, Mn, Co, Ni, Cu, Zn

trivalent cations: Al, Mn, Fe, Co, Ni, Cr, Ga.

One major characteristic of LDHs is that in most cases, only weak bounding occurs between the interlamellar ions and the layers. A great variety of anionic species can therefore be located between the layers during the formation of the lamellar structure, or by further anionic exchange. These anions can be:

- halides: fluoride, chloride,...
- oxo-anions: carbonate, nitrate, sulphate, bromate,...
- organic anions: carboxylates, phosphonates, alkyl sulphates,...

In addition to anions and water molecules, the interlamellar domains can contain other neutral species.

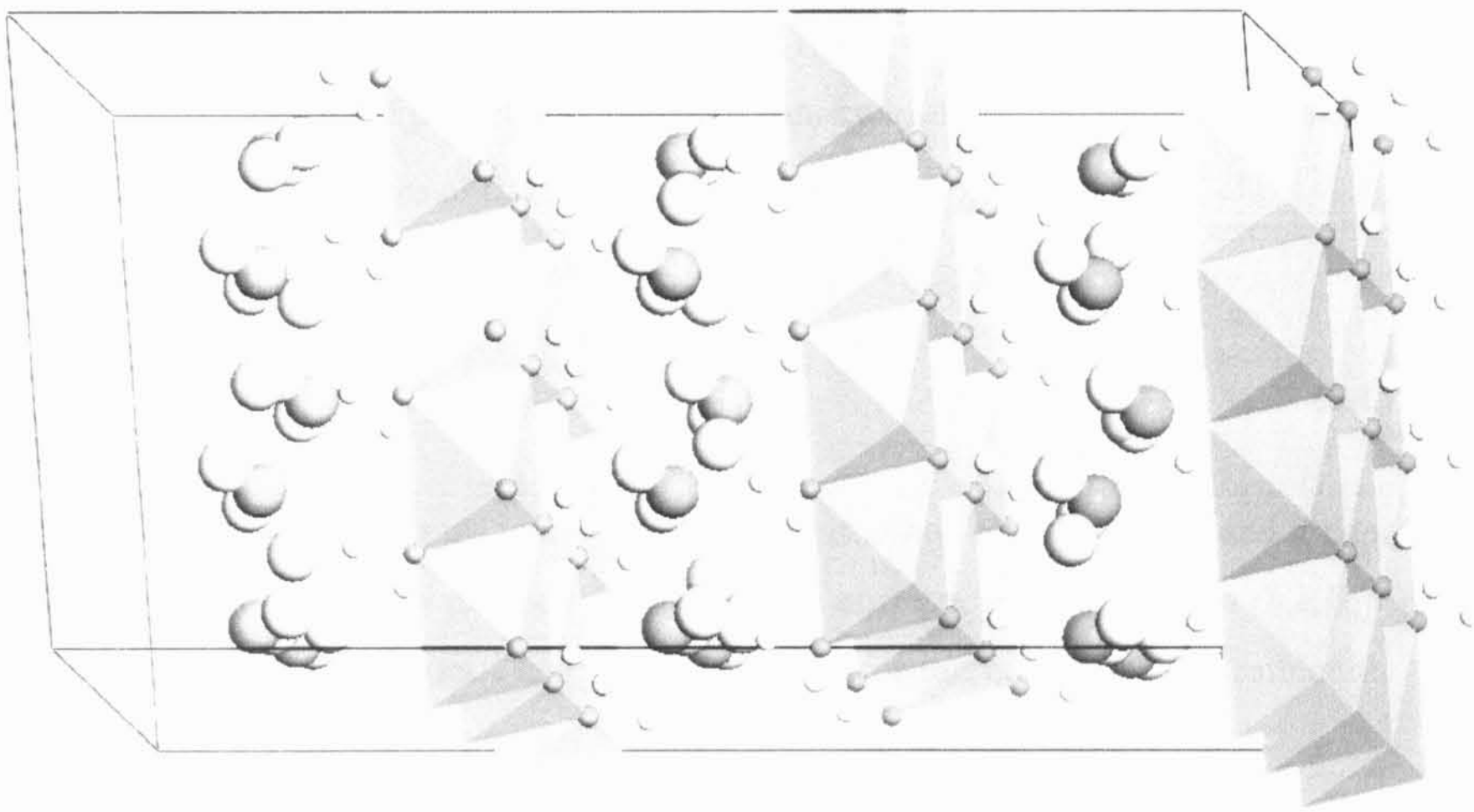

Fig 2.1. Zn_4-Al_2-Cl_2 Layered Double Hydroxide. The grey octahedra contain Zn atoms; the violet ones contain Al atoms. Small red and white balls represent OH groups of the layers, the big red and white balls represent oxygen and hydrogen atoms of the interlayer water molecules. The green balls represent exchangeable chloride anions.

The structure of the interlayer space is more difficult to characterize than the structure of the layers. With small anionic species, such as halides and carbonates and up to sulphate – containing LDHs with a basal spacing of 11 Å, a regular stacking of the layers is observed in the X-ray diffraction patterns. With bulky anions, the stacking of the layers displays in most cases no more long-range ordering (turbostatic effect) [16] and the diffractograms show only lines relative to the basal spacing and to the structure of the layers.

Natural and synthetic LDHs usually crystallize in two polytype structures, one with a two-layer hexagonal stacking sequence (polytype 2H, space group P63/mmc, or P63/mcm) and one with a three-layer rhombohedral sequence (polytype 3R) which is represented by space group *R-3m*.

Since the end of 1960s, an increasing interest is being given to LDHs in many fields such as structural characterization [17], electrochemical and magnetic properties [18, 19], catalysis [20, 21], pharmaceutical applications [22, 23], ecology [24] etc.

3. X-ray diffraction

In diffraction experiments, intensities and positions of reflections are measured. From the position of the reflection, its index triple (*h k l*) can be determined and the appropriate intensity assigned to it [25]. The amplitude of intensity of diffracted radiation by one unit cell is proportional to the square of the structure factor: $I_{(h,k,l)} \approx F_{(h,k,l)} F^{*}_{(h,k,l)}$.

The expression for the structure factor is

$$F_{(h,k,l)} = \sum_{j=1}^{n} f_{(j)} \exp\left[2\pi \cdot i(hx_{(j)} + ky_{(j)} + lz_{(j)})\right], \qquad (3.1)$$

where n is the number of atoms in unit cell, $f_{(j)}$ is scattering factor of atom j and it depends on the kind of atom and on the diffraction angle of the corresponding reflection *(h,k,l)*; x,y,z are fractional coordinates of atom j and h,k,l are indices of the corresponding reflection. If the structure is known, the expression for the structure factor is

$$F_{h,k,l} = \int_{V} \rho(\vec{r})\, e^{2\pi i \vec{H}\vec{r}}\, dV\,, \qquad (3.2)$$

where V is volume of unit cell, $\rho(\vec{r})$ is electron density in unit cell, $\vec{H} = ha^{*} + kb^{*} + lc^{*}$ is a reciprocal lattice vector and $\vec{r}$ is a direct lattice vector. The aim of the crystallographic studies

is to find out the structure from the measured intensity, i.e. from the experimentally obtained structure factor. The way to look into the electron density is an inverse Fourier transformation:

$$\rho_{(x,y,z)} = \frac{1}{V}\sum_{h}\sum_{k}\sum_{l}\left|F_{(h,k,l)}\right|\exp\left[-2\pi\cdot i\left(hx+ky+lz\right)\right]. \qquad (3.3)$$

The problem is that only the magnitude of complex structure factors is known, i.e. one does not know the phase and the next is to find it out by solving the Phase Problem. A difficulty leading to an impossibility of using the structure determination based on X-ray diffraction only is that the intercalated layered double hydroxides usually exhibit a disorder in the positions and orientations of the guest anions with respect to LDH layers and they usually exhibit a layer stacking disorder. A typical diffraction pattern of intercalated LDH has *00l* reflections and it contains typical broaden *hk*-bands that are characteristic for LDH structure. Generally, the X-ray diffraction profile is affected by other factors such as: for example (i) the size of the particles, (ii) rudeness of the surface of the layers, (iii) quality of crystalinity and temperature [26]. We can determine the interlayer distance of the intercalated LDH and by comparing the experimental and the calculated X-ray diffraction pattern obtained by modeling, we can determine the arrangement in the interlayer space of LDH.

4. Molecular modeling

Molecular modeling is based on the optimization of the structure and bonding geometry using energy minimization where the energy of the system is described by an empirical forcefield. Molecular simulations are often used when the investigated systems are too large for ab initio calculations and for the crystal structures that exhibit a certain degree of disorder and cannot be determined experimentally by using direct diffraction methods as it was mentioned above. Molecular simulations are divided into two parts: molecular mechanics and molecular dynamics. All the calculations in this work were done in *Cerius*^{2} modeling environment [27]. More information about molecular simulations can be found in [28].

4.1 Molecular mechanics

Molecular mechanics is based on the approximation which assumes that the motions of the electrons and the nuclei are independent. The electrons are considered to be fixed to the nuclei

during the calculations and only positions of the nuclei are calculated. This is in the contrast with the quantum mechanics attitude.

In molecular mechanics, all forces between the atoms are calculated using classical mechanical approach. The atoms are described as balls and they are connected by bonds with different elasticity. The interactions between atoms are described by potential energy functions in the selected force field. The force field parameters are usually based on experimental data and the quality of calculations in the given force field are strongly dependent on the reliability of the potential energy functions and on corresponding force field parameters.

4.1.1 Potential energy functions

It is common practice to represent the total energy of a system by a set of potential energy functions, including bonded (E_b) and nonbonded (E_{nb}) interactions.

$$E_{total} = E_b + E_{nb} \tag{4.1}$$

The bonded terms are comparable with the terms used in spectroscopy, and they consist of two-body interactions (bonding energy E_{bond}), three-body interactions (valence angle energy E_{ang}) and four-body interactions (torsion angle energy E_{tor} and inversion E_{inv}):

$$E_b = E_{bond} + E_{ang} + E_{tor} + E_{inv}. \tag{4.2}$$

The nonbonded terms consist of van der Waals (E_{vdW}), electrostatic (E_{elst}) and hydrogen bonding (E_{hb}) terms:

$$E_{nb} = E_{vdW} + E_{elst} + E_{hb}. \tag{4.3}$$

4.1.2 Bonded interactions

Bond length deformation

The simplified approach used in molecular mechanics is to describe bond stretching as a mechanical spring whose force constant is strong for small interatomic distances r and weak for large ones. One possible way how to describe it is a Morse potential:

$$E_{bond} = D\left[1 - \exp\left(-\alpha\left(r - r_0\right)\right)\right]^2, \tag{4.4}$$

where r_0 is the ideal bond distance, α describes the curvature and D the depth of the potential function. The disadvantage of using a Morse function in empirical force field calculations is that two potential functions and three parameters are involved and it causes an increase the time requirement for the minimization process. A Morse function may be mimicked by a Taylor expansion, where the first term (quadratic) describes a harmonic potential and higher-order terms are included as inharmonic corrections. The quadratic term is a good approximation of the bond stretching function near the energy minimum.

Valence angle deformation

For organic molecules valence angle bending is usually described by a harmonic potential E_{ang}:

$$E_{ang} = \frac{1}{2} k_\theta (\theta - \theta_0)^2, \qquad (4.5)$$

where θ is the angle between atoms i, j, k, θ_0 is the ideal bond angle, k_θ is a force constant.

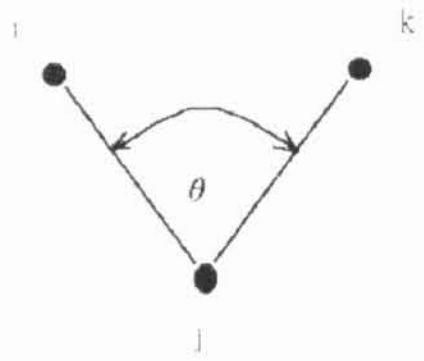

Fig 4.1. Valence angle deformation

The fact that molecular mechanics is a well-developed tool for organic molecules while coordination compounds have been modeled less frequently in the past is partly related to problems in being able to model reliably the angles at the transition metal centers. In organic compounds sp^3, sp^2 and sp hybrids lead to relatively stiff angles of 109.5°, 120° and 180°, respectively, which are conveniently modeled with functions of the type (4.5). In contrast, metal ions are more complex. A number of functions have been proposed to model the valence angles around the metals. The molecular mechanics forcefield Dreiding, based on a generic force field, uses a harmonic cosine function

$$E_{ang} = \frac{1}{2} k_\theta^c \left(\cos\theta_{ijk} - \cos\theta_0\right)^2, \qquad (4.6)$$

where k_{ijk}^{c} is a force constant, θ_{ijk} is the angle between atoms *i*, *j*, *k* and θ_0 is the ideal bond angle.

Sometimes a Urey-Bradley potential function is added to the expression E_{ang}. It describes the bonded energy of the atoms *i* and *j* that are bonded to their common atom *k*. The Urey-Bradley potential term can be expressed in the simplest form as follows:

$$E_{UB} = \frac{1}{2} k_{UB0} \left(r_{ij} - r_0 \right)^2 + k_{UB1} \left(r_{ij} - r_0 \right), \tag{4.7}$$

where k_{UB0} and k_{UB1} are force constants and r_{ij} is a bond distance between the atoms *i* and *j*, r_0 is the ideal distance between the atoms *i* and *j*.

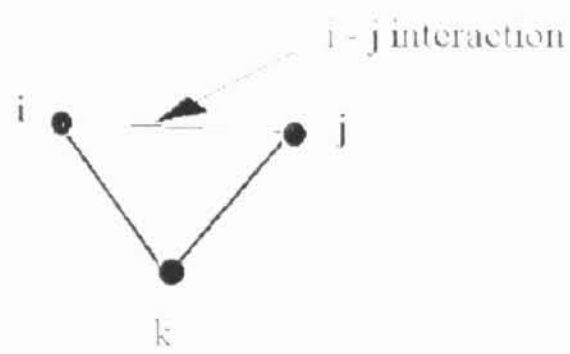

Fig 4.2. Illustration to Urey-Bradley potential

Torsion angle deformation

Torsion rotations around single and multiple bonds are different processes. In a multiple bond, a torsion rotation results in the transformation of one isomer into another. Rotation around single bonds leads to interconversion of conformers. It is common practice to describe torsion rotations around single bonds and those around multiple bonds with the same type of potential function but with very different force constants. The function must be able to describe multiple minima. Generally, a Fourier expansion of the torsion angle ϕ with only cosine terms is used:

$$E_{tor} = \sum_n \frac{1}{2} k_n \left(1 + \cos\left(m_n \left(\phi - \phi_0 \right) \right) \right), \tag{4.8}$$

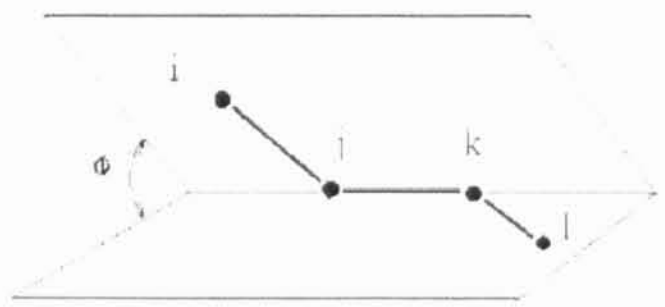

Fig 4.3. Torsion angle deformation around the *j-k* bond

where the constant k_n represents a rotational barrier, m_n is the multiplicity and ϕ_0 is a phase shift which only has to be considered if only one cosine term is included.

Inversions

An inversion term describes the bonding geometry of four atoms *i*, *j*, *k*, *l* and characterizes the deviation from a planar arrangement. There are three various types of inversions:

- umbrella inversion

$$E_u = \frac{1}{2} k_u \left(\cos\omega - \cos\omega_0\right)^2, \tag{4.9}$$

where k_u is a force constant, ω is the angle between the *ijk* plane and the axis *il*, ω_0 is the equilibrium value of this angle.

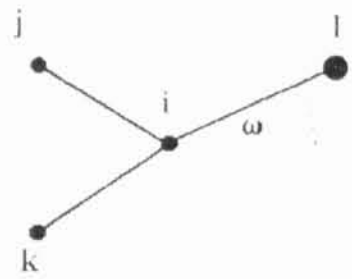

Fig 4.4. Umbrella inversion

- amber inversion

$$E_a = \frac{1}{2} k_a \cos\left[n\left(\psi - \psi_0\right)\right], \tag{4.10}$$

where k_a is an energetic rotational barrier, n periodicity, ψ is the angle between the *jil* and *kil* planes and ψ_0 is the equilibrium value of this angle.

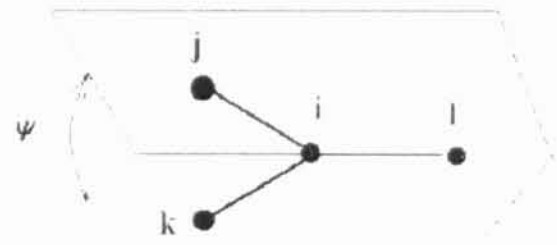

Fig 4.5. Amber inversion

- charm inversion

$$E_{ch} = \frac{1}{2} k_\sigma \left(\psi - \psi_0\right)^2, \tag{4.11}$$

where k_σ is a force constant, ψ is the angle between the *ijk* and the *ljk* planes, ψ_0 is the equilibrium value of this angle.

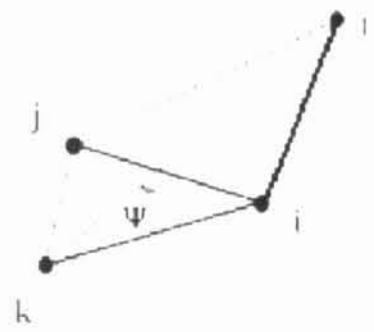

Fig 4.6. Charm inversion

A separation of the bonded interactions into bond stretching (E_{bond}), angle bending (E_{ang}), torsion angle rotation (E_{tor}) and inversions (E_{inv}) is only possible if these terms are not coupled, and this is the most likely if the force constants are very different. In cases where this requirement is violated, corrections have to be added. This can be done by the inclusion of cross-terms (coupled terms) which describe bond or angle distortions caused by nearby atoms. The crossterms include the following coupled terms: stretch-stretch, stretch-bend-stretch, bend-bend, torsion-stretch, torsion-bend-bend, bend-torsion-bend and stretch-torsion-stretch.

4.1.3 Non-bonded interactions

Van der Waals interactions

Various interactions, such as those of permanent electric dipoles, permanent multipoles, and short-lived multipoles, are assembled in the van der Waals term. At distances below the van der Waals radius, the atoms repel each other; above it they attract each other. The attractive force is modeled by a $1/r^6$ term, while various possibilities exist for the repulsion. The van der Waals interaction can be calculated by a Lenard-Jones potential eq. (4.12) or by a Buckingham potential eq. (4.13)

$$E_{vdW} = \frac{A}{r_{ij}^{12}} - \frac{C}{r_{ij}^{6}}, \tag{4.12}$$

$$E_{vdW} = A e^{-Br_{ij}} - \frac{C}{r_{ij}^{6}}, \tag{4.13}$$

where r_{ij} is the distance of the atoms i and j , the capital letters are constants.

Electrostatic interactions

In this work, charges were calculated by using Charge equilibrium approach [29]. The Ewald summation method is used to calculate the Coulomb energy [30]. The real space Coulomb sum is divided into a quickly converging modified real-space sum and a summation in a reciprocal space. The division is specified by three parameters: the Ewald sum constant, the real-space sum cutoff, the reciprocal-space sum cutoff. The Ewald sum constant controls the division of a work between the real- and reciprocal-space sums. The bigger the Ewald sum constant is, the more quickly convergent the real-space sum is, but the more slowly convergent the reciprocal-space sum is.

Hydrogen bonding interactions

The function most used for hydrogen bonding interactions is a two-parameter function with a repulsive term that decreases with d^{12} and an attractive term that decreases with d^{10}:

$$E_{hb} = \frac{F}{d_{ij}^{12}} - \frac{G}{d_{ij}^{10}}, \tag{4.14}$$

where F and G are constants and d_{ij} is a donor-acceptor distance.

4.2 Minimization algorithms

The minimization of a system is done in two steps. Firstly, an equation describing the energy of the system as a function of its coordinates is defined and evaluated for a given conformation. Next, the conformation is adjusted to a lower energy value of the target function. The number of iterations depends on the nature of the algorithm, the form of the target function and the size of the system.

Line search

The major implicit component of most minimization algorithms is the so-called line search that generally changes the coordinates of the atoms to the new ones with lower energy. Line search amounts to a one-dimensional minimization along a direction vector determined at each iteration. The derivative vector from the initial point of the energy surface defines the line search direction. This vector does not lead generally to the minimum, but the algorithm tries to find a minimum on this line and after that, it assigns a new vector which is

perpendicular to the previous one. It occurs for all iterations. The line search provides an efficient path to the minimum for approximately quadratic surfaces.

Minimization algorithms used in MSI's simulations are: steepest descents, conjugate gradient and Newton-Rapson methods.

Steepest descents

In the steepest descents method, the line search direction is defined along the direction of the local downhill gradient. Each line search produces a new direction that is perpendicular to the previous gradient $\nabla E(x_i, y_i)$, however, the directions can oscillate along the way to the minimum. This inefficient behavior is characteristic for steepest descents on energy surfaces having narrow valleys. If the line search was eliminated and the positions were updated any time that the trial point along the gradient had a lower energy the number of function evaluations would dramatically decrease. Furthermore, by constantly changing the direction to match the current gradient, oscillations along the minimization path might be damped. Each line uses, at most, two function evaluations if the trial point has a higher energy, the step size is adjusted downward and a new trial point is generated. Convergence of steepest descents is slow near the minimum because the gradient approaches to zero, but the method is extremely robust when the gradients are large and the configurations are far from the minimum, so the steepest descents should be used for the first 10 -100 steps of minimization.

Conjugate gradient

The steepest-descents method converges slowly near the minimum and each line search deviates from the ideal direction to the minimum. Successive line search does not correct for this deviations efficiently because each direction must be orthogonal to the previous one. The conjugate gradient method produces a set of mutually conjugate directions such that each successive step continually refines the direction towards to the minimum.

In conjugate gradient, the new direction vector $\mathbf{h}_{i+1}$ leading from point i+1 is computed by adding the gradient at point i+1, $\mathbf{g}_{i+1}$ to the previous direction $\mathbf{h}_i$ scaled by a constant γ:

$$\mathbf{h}_{i+1} = \mathbf{g}_{i+1} + \gamma_i \mathbf{h}_i, \qquad (4.15)$$

where γ is a scalar that can be defined in two ways. In the Polak- Ribiere method, γ is defined as

$$\gamma_i = \frac{(\mathbf{g}_{i+1} - \mathbf{g}_i)\mathbf{g}_{i+1}}{\mathbf{g}_i \mathbf{g}_i} \tag{4.16}$$

and in the Fletcher – Reeves method γ is defined as

$$\gamma_i = \frac{\mathbf{g}_{i+1}\mathbf{g}_{i+1}}{\mathbf{g}_i \mathbf{g}_i}. \tag{4.17}$$

The two conjugate gradient methods have similar characteristics; one or other might behave better in certain cases. This direction is then used in the place of the gradient in the steepest descents. The algorithm produces a set of mutually orthogonal gradients and a set of mutually orthogonal directions. The method converges in approximately N steps, where N is the number of degrees of freedom. Conjugate gradients are the method of choice for large systems because only the previous $3N$ gradients and directions have to be stored. The disadvantage of this method is that the time per iteration may be longer in comparison with the steepest descents because of the more complete line search is done with more function evaluations. Longer calculating time is compensated by more efficient convergence to the minimum.

Newton-Raphson methods

As a rule, N^2 independent data are required to numerically solve a harmonic function with N variables. If one can exploite second-derivative information, a minimization could ideally converge in one step, because second derivative is an N x N matrix. This is the principle behind the variable metric minimization algorithms, of which Newton-Raphson is the most used. In addition to using the gradient to identify a search direction, the curvature of the function (second derivative) is also used to predict, where the function passes through a minimum along that direction. The inverse of the second-derivative matrix multiplied by the gradient obtains a vector that translates directly to the nearest minimum. This is expressed mathematically as

$$\mathbf{r}_{\min} = \mathbf{r}_0 - \mathbf{A}^{-1}(\mathbf{r}_0).\nabla E(\mathbf{r}_0), \tag{4.18}$$

where $\mathbf{r}_{\min}$ is the predicted minimum, $\mathbf{r}_0$ is an arbitrary starting point, $\mathbf{A}(\mathbf{r}_0)$ is the matrix of second partial derivatives of the energy with respect to the coordinates at $\mathbf{r}_0$ and $\nabla E(\mathbf{r}_0)$ is the gradient of the potential energy at $\mathbf{r}_0$.

The molecular energy surface is generally not harmonic, so the minimum energy structure cannot be determined with one Newton-Raphson step. Instead, the algorithm must be applied iteratively:

$$\mathbf{r}_i = \mathbf{r}_{i-1} - \mathbf{A}^{-1}(\mathbf{r}_{i-1}).\nabla E(\mathbf{r}_{i-1}). \qquad (4.19)$$

This algorithm appears to be very elegant, but its application to molecular modeling has several drawbacks. First, the terms in the second derivatives matrix are difficult to derive and are computationally costly for molecular force fields. Furthermore, when a structure is far from the minimum the minimization can become unstable because of the inharmonicity of the energy surface and it can diverge rapidly if the initial forces are too high. Finally, calculating, inverting, and storing an N x N matrix for a large system can become unwieldy. Pure Newton-Raphson is reserved primarily for cases where rapid convergence to an extremely precise minimum is required.

4.3 Molecular dynamics

While minimization computes the forces on the atoms and changes their positions to minimize the interaction energies, dynamics computes forces and moves atoms in response to the forces. Molecular dynamics solves the classical equations of motion for a system of N atoms interacting according to a potential energy force field. Dynamics simulations are useful for studies of the time evolution of variety of systems at nonzero temperatures, for example, biological molecules, polymers, or catalytic materials, crystals, aqueous solutions, or the gas phase.

The major applications of molecular dynamics are:

- **Performing conformational searches**

During dynamics simulations, a system undergoes conformational and momentum changes so that different parts of the phase space accessible to the molecules can be explored.

- **Generating statistical ensembles**

Molecular dynamics allows us to generate statistical ensembles from which various energetic, thermodynamic, structural and dynamic properties can be calculated.

- **Studying the motions of molecules**

The thought of intermolecular collisions and conformational variations is always present. Binding of substrates by proteins, folding of proteins and peptides into unique shapes, dynamic behavior of polymers, and chemical reactions themselves would be inconceivable without the concept of molecular motion. Studies of molecular motions can be used to derive properties such as diffusion coefficients.

Integration algorithms

Molecular dynamics solves Newton's equation of motion

$$\mathbf{F}_i(t) = m_i a_i(t). \tag{4.20}$$

where $\mathbf{F}_i$ is the force, m_i is the mass, and a_i is the acceleration of the atom i.

The force on the atom i can be computed directly from the derivative of the potential energy V with respect to the coordinates $\mathbf{r}_i$:

$$\frac{\partial V}{\partial \mathbf{r}_i} = m_i \frac{\partial^2 \mathbf{r}_i}{\partial t_i^2}. \tag{4.21}$$

Classical equations of motion are deterministic. That is, once the initial coordinates and velocities are known, the coordinates and velocities at a later time can be determined. Although the initial coordinates are determined in the input file or from a previous operation such as minimization, the initial velocities are randomly generated on the base of Gauss distribution at the beginning of a dynamics run, according to the desired temperature. Therefore, dynamics run cannot be repeated exactly. The algorithm which integrates the equations of motion is called the integrator. Molecular dynamics is usually applied to a large system, so the energy evaluation is time consuming and the memory requirement is large. To generate the correct statistical ensemble, energy conservation is also important. The basic criteria for a good integrator in algorithms are as follows:

- It should be fast, ideally requiring only one energy evaluation per time step.
- It should require little computer memory.
- It should permit to use of a relatively long time step.
- It must show a good conservation of energy.

The *Cerius*^{2} dynamics simulation module uses the Verlet leapfrog integrator, whose variants are used widely in molecular dynamics because it requires only one energy evaluation per step, requires only modest memory, and allows a relatively large timestep to be used.

The Verlet leapfrog algorithm is as follows:

Given $\mathbf{r}(t)$, $\mathbf{v}(t - \Delta t/2)$ and $\mathbf{a}(t)$, which are the position, velocity, and acceleration at times t, and $t - \Delta t/2$, compute:

$$\mathbf{v}\left(t + \frac{1}{2}\Delta t\right) = \mathbf{v}\left(t - \frac{1}{2}\Delta t\right) + \Delta t\,\mathbf{a}(t), \tag{4.22}$$

$$\mathbf{r}(t + \Delta t) = \mathbf{r}(t) + \Delta t\,\mathbf{v}\left(t + \frac{1}{2}\Delta t\right), \tag{4.23}$$

$$\mathbf{a}(t + \Delta t) = \frac{\mathbf{f}(t + \Delta t)}{m}, \tag{4.24}$$

where $\mathbf{f}(t + \Delta t)$ is evaluated from $-dV/d\mathbf{r}$ at $\mathbf{r}(t + \Delta t)$.

The disadvantage of the Verlet leapfrog method is that the positions and velocities are calculated half a timestep of synchrony.

Δt is called the integration timestep and it is very important parameter in the integration algorithm. Large timestep causes instability and inaccuracy in the integration process. In most molecular systems, the main limitation is the highest-frequency motion that must be considered. The highest vibrational frequency is usually given by frequency of C – H bond stretching, whose period is of the order of 10 fs. So, the integration timestep should be about 0.5 – 1 fs.

4.3.1 NVT ensemble

The constant number of particles, constant volume, constant temperature ensemble (NVT) was used in this work. NVT ensemble is also referred to as canonical ensemble and it is obtained by controlling the thermodynamic temperature. Direct temperature scaling should be used only during the initialization stage, since it does not produce a true canonical ensemble.

The NVT ensemble calculations are used when conformational searches of molecules are carried out in a vacuum without periodic boundary conditions. Even when periodic boundary conditions are used, if pressure is not a significant factor, NVT ensemble provides the

advantage of less perturbation of the trajectory, due to the absence of coupling to a pressure bath.

4.3.2 Temperature

Temperature is a state variable that specifies the thermodynamic state of the system and is an important parameter in dynamics simulations. It is related to the microscopic description of molecular simulations through the kinetic energy which is calculated from the atomic velocities.

The temperature and the distribution of atomic velocities in a system are related through the Maxwell-Boltzmann equation:

$$f(v)\,dv = \left(\frac{m}{2\pi kT}\right)^{3/2} e^{-\frac{mv^2}{2kT}} 4\pi v^2\,dv, \qquad (4.25)$$

where v is molecular velocity, m mass of molecule, T represents thermodynamic temperature and k is Boltzmann constant.

The following formula expresses the probability $f(v)$ that a molecule of mass m has a velocity of v when it is at temperature T. The x, y, z components of the velocities have Gaussian distributions:

$$g(v_x)\,dv_x = \left(\frac{m}{2\pi kT}\right)^{1/2} e^{-\frac{mv_x^2}{2kT}}\,dv_x. \qquad (4.26)$$

The initial velocities are generated from the Gaussian distribution of v_x, v_y, v_z. The Gaussian distribution is generated from a random number generator and a random number seed.

Temperature is related to the average kinetic energy of the system through the equipartition principle which states that every degree of freedom, which appears as a squared term in the Hamiltonian, has an average energy of $kT/2$ associated with it.

4.3.3 Quenched dynamics

In quenched dynamics, periods of dynamics are followed by a quench period in which the structure is minimized. The minimized structure can be written to a trajectory file, and dynamics continues with the prequenched structure. Quenched dynamics is a way to search conformational space for low-energy structures.

5. Results

The advantages of molecular modeling for small systems with hundreds of atoms lies in a fact that the simulation of these systems is not too computer time consuming and many different methods and strategies of molecular modeling can be fast tested in a relatively short time. Once the suitable computational strategy is worked out one can use it for structure determination of much larger systems with similar parameters.

Thus, the main goal of this work was:

1/ to test different simulation strategies for the geometry optimization of the models and by using various combination of constraints involved in the calculating software to obtain a faster convergent results and also to spare the computing time,

2/ to investigate and to describe structure models of LDH intercalated with benzoate and LDH intercalated with benzoate-derivates (p-methyl and p-bromobenzoate) on the base of the similarity of the calculated and the experimental diffraction pattern. It means to obtain an agreement of the experimental and the calculated interlayer distance value, to obtain a good similarity of the part of X-ray diffraction profile related to basal reflections and to eliminate undesirable reflections in the calculated diffraction pattern which can be caused by a forced periodicity.

The LDH layers were constructed in *Crystal Builder* [27] module according to the crystallographic data. In the case of Zn-Al LDH intercalated with benzoate it was gained from Rietveld refinement at the cooperative workplace in Perugia, Italy: Trigonal cell system, space group R-3m. Cell parameters: $a = b = 3.07598$ Å, $c = 23.2048$ Å. The atomic fraction coordinates are shown in the table 1.

These atomic fraction coordinates were used for constructing the cell of Mg_4-Al_2 LDH + p-methyl and p-bromobenzoate intercalate and the cell parameters were taken from [31]. The guest anions were constructed in *3-D Sketcher* module [27].

Table 1. Atomic fraction coordinates of the elements of LDH layer.

Element	x/a	y/b	z/c
Zn (Al,Mg)	0	0	0
O	0	0	0.377

The LDH intercalates consist of inorganic part that is formed by Zn or Mg and Al atoms in the layers. A lot of forcefields are available to describe many types of special species like DNA, polymers, glasses etc. The only forcefield which was able to describe all the atoms in the structure models of LDH intercalates was *Universal* forcefield [32] and it was used for all the calculations.

3 types of minimization strategy were evaluated:

1/ The unit cell parameters and the positions of all the atoms in the LDH layers are fixed and the atomic positions of all the species in the interlayer space are variable. This type of constraints does not enable to investigate the dependence of the interlayer distance on the arrangement of the species in the interlayer space.

In the case of molecular modeling of such intercalates that have very broaden basal reflections the value of interlayer distance is the only parameter that connects the modeling and the experiment. Therefore this constraint is unusable because one cannot say that a certain arrangement of the interlayer space is probable than other because the interlayer distance is not optimized. On the other hand, this constraint leads to a very quick convergence of energy of the minimized structure.

2/ The unit cell parameters and all the atomic positions in the model are variable. This strategy leads to the slowest convergence of the energy because there are no constraints. This strategy enables us to investigate a possible distortion of the LDH layers in the model and changes in the LDH layer itself, for example, the bond length distance and valence angle changes. As if we use *Universal* forcefield these changes will not be described properly. They would be better described if special forcefields for clay minerals were derived. In contrast of this, we found out that this strategy leads to incorrect results in the case of LDH – the interlayer distance does not agree with the experimental one at all and the structure of interlayer space is very different from the results obtained by other strategies.

3/ The layers are kept as „rigid units" i.e. the mutual position of the atoms in the layers are fixed and the layers as rigid units can move in a horizontal and in a vertical direction with respect to each other. The corresponding cell parameters are variable (if *x*-axis is perpendicular to the layers the parameters *c*, *alpha* and *beta* are variable and basal reflections in the calculated X-ray diffraction pattern are labelled as (*l 0 0*)). This strategy leads to a faster convergence than strategy no. 2 and the establishment of the „rigid bodies" agrees with

the fact that the structure of the host layers remains unchanged after the intercalation or the changes are small. In addition, one can investigate dependence of the interlayer distance value on the arrangement of the species in the interlayer space. It is also possible to look into a layer stacking disorder of the structure model and into the dependence of the interlayer distance and a diffraction pattern profile of the intercalate on the concentration of the species in the interlayer space. This strategy was used in our calculations.

Molecular dynamics

A NVT (constant number of atoms, constant volume and constant temperature) statistical ensemble was used in molecular dynamics. In this statistical ensemble the layers are kept fixed, the cell parameters are not allowed to change and only the geometry of the interlayer arrangement is optimized. It enables us to investigate the dependence of the total crystal energy on the arrangement of the species in the interlayer space and the molecular dynamics calculations are not too time consuming.

Solved structures:

In the following pages, structure models of LDH + benzoate intercalate and calculated X-ray diffraction patterns are shown. The experimental X-ray diffraction pattern of the intercalate is shown in the paper I.- fig 1. The values of the 2θ angle and the corresponding *l 0 0* basal reflections are presented in the table 2.

Table 2. 2θ angle and corresponding *l 0 0* basal reflections.

2θ /°	5.84	11.48	17.20	23.06	28.85
l 0 0	3 0 0	6 0 0	9 0 0	12 0 0	15 0 0

Some types of different arrangements of the species in the interlayer space are shown in the figures 5.1 and 5.3. The figures 5.1 and 5.2 show a structure model and the X-ray diffraction pattern with a parallel arrangement of benzoate anions in the interlayer space and with water molecules freely distributed in the interlayer space.

In the figures 5.3 and 5.4 a model with a tilted arrangement of the guest anions in the interlayer space and its X-ray powder diffraction is shown.

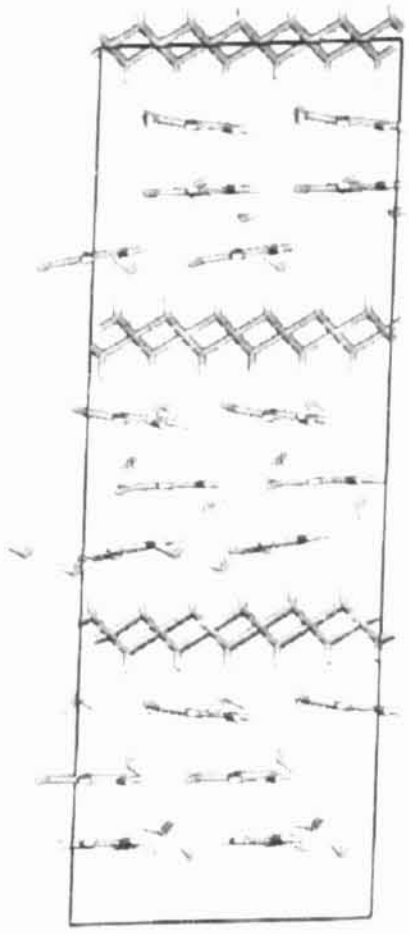

Fig. 5.1. A model with parallel arrangement of the guest anions in the interlayer space.

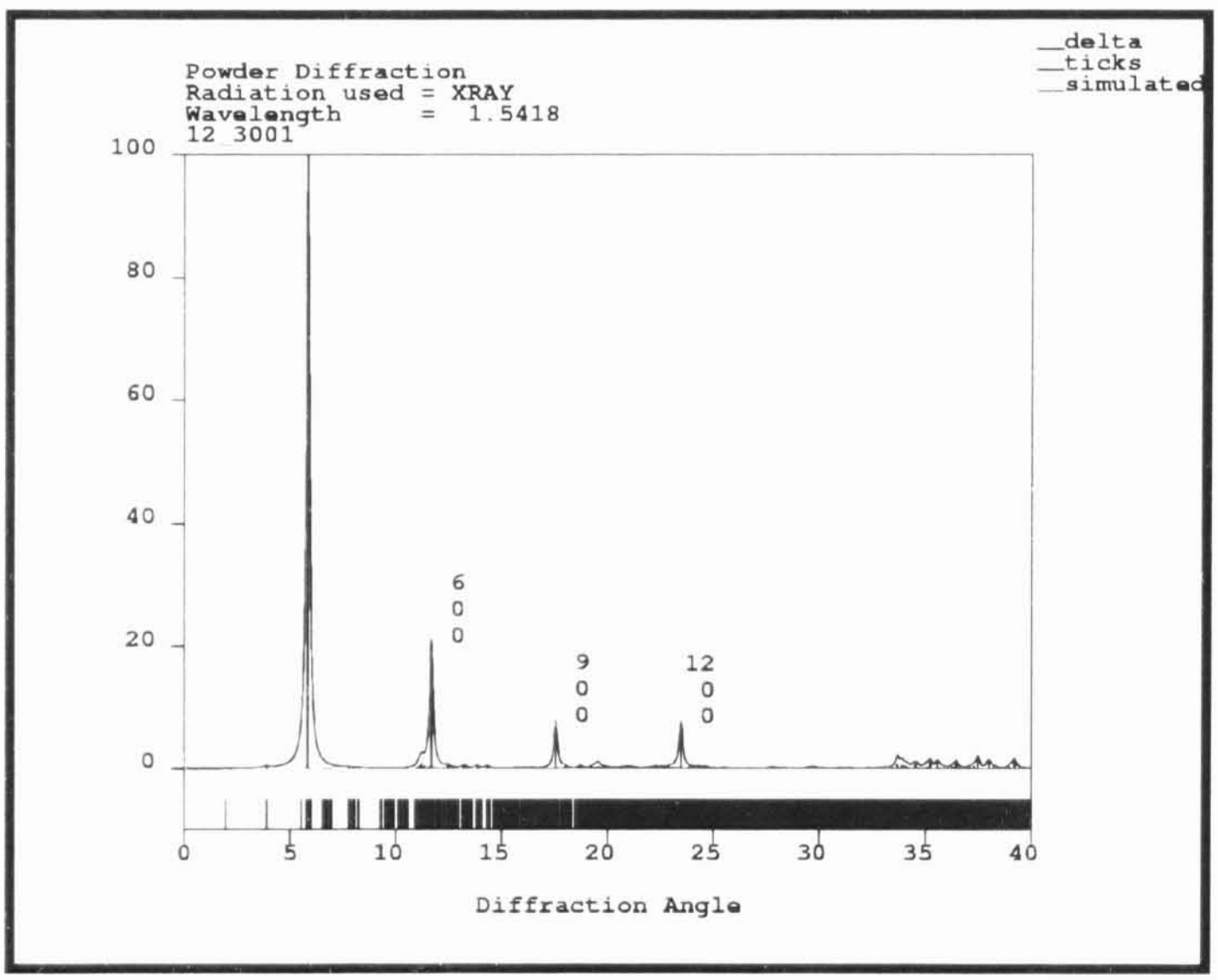

Fig. 5.2. Calculated X-ray diffraction pattern of the parallel arrangement of the guests in the interlayer space.

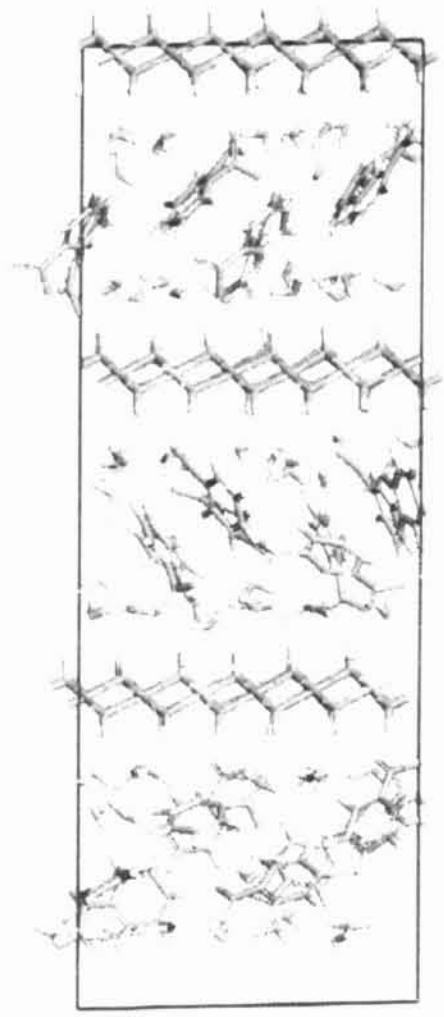

Fig. 5.3. A model with tilted arrangement of the guest anions in the interlayer space.

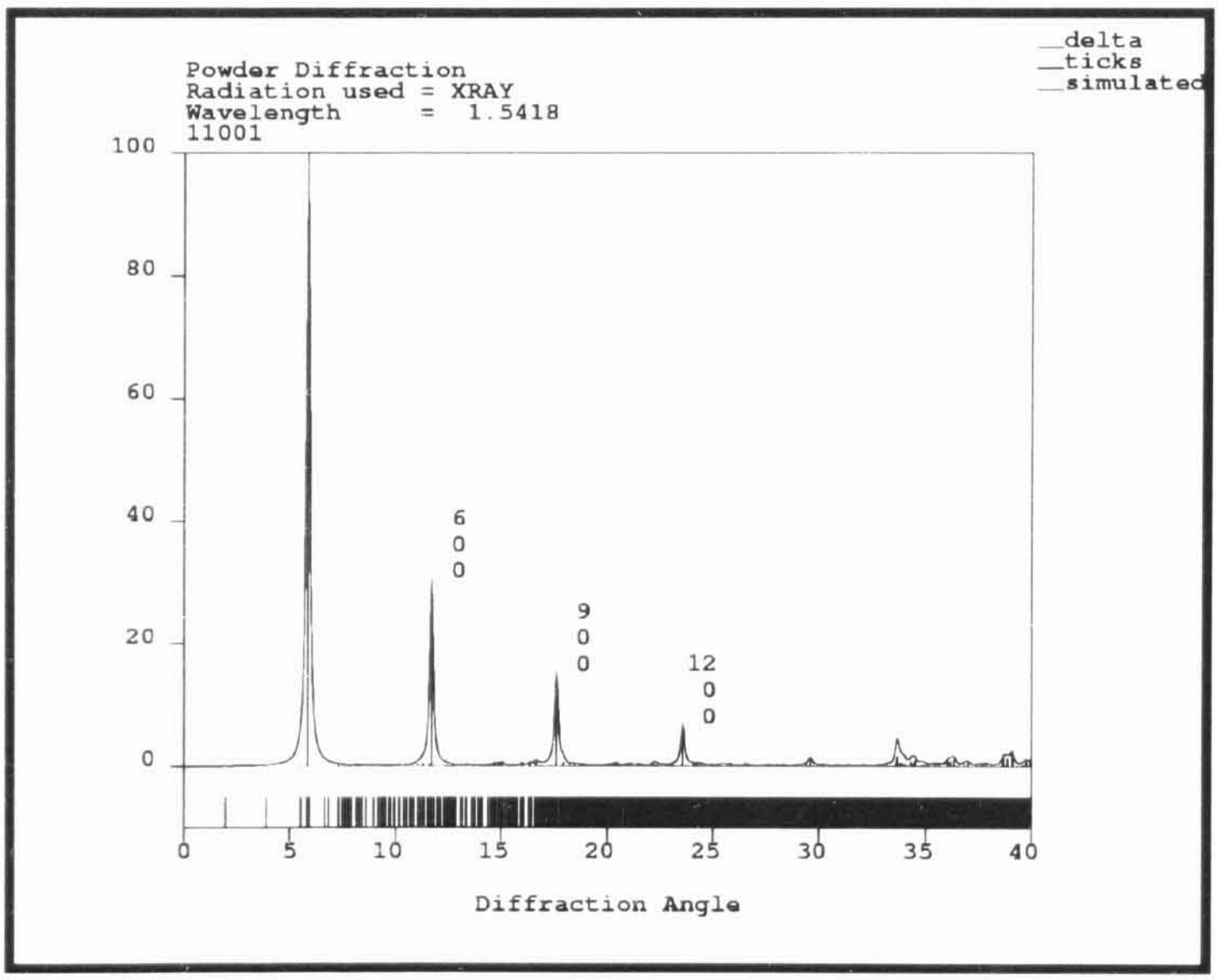

Fig. 5.4. Calculated X-ray diffraction pattern of the tilted arrangement of the guests in the interlayer space.

One can see that by comparing the calculated X-ray diffraction patterns and the structure models of LDH intercalated with benzoate we can investigate the influence of different arrangement of the interlayer space on the X-ray diffraction profile. We can see that the arrangement of the interlayer space significantly affects the ratio of the intensities of (9 0 0) and (12 0 0) reflections. In addition in the case of parallel arrangement of the guests the (15 0 0) reflection is missing (2θ for (15 0 0) reflection is 29.0°) in the calculated X-ray diffraction pattern, which leads to a disagreement with the experimental diffraction pattern. In the tilted arrangement of the guests the (15 0 0) reflection is present but the ratio of intensities of (9 0 0) and (12 0 0) reflections is not satisfactory. The most probable structure model is the one with the nearly perpendicular arrangement of the guests where the ring planes of the guests keep the parquet arrangement as it is shown in the paper I-fig 3a. Its X-ray diffraction profile resembles the best of the experimental X-ray diffraction profile.

When the arrangement of guests in the interlayer space was solved we carried out a simulation of the arrangement of the interlayer space of LDH intercalated with p-bromobenzoate and p-methylbenzoate. The basal reflections for LDH + benzoate-derivatives intercalates are labeled in the experimental diffraction pattern in paper II-fig 2.

We found out that the added CH_3 groups and the Br atoms in p-positions of benzoate rings influence the arrangement of the guests in the interlayer space. In the case of LDH intercalated with p-methylbenzoate the guest tend to be situated in disordered rows as it is shown in paper II.-fig 3b and in the case of LDH intercalated with p-bromobenzoate there is a total disorientation of the guests in the interlayer space, see paper II.-fig 4b.

We found out that interlayer water has a significant influence on the X-ray diffraction profile in the cases of all intercalates. Different arrangements of water molecules lead to different intensities of (12 0 0) reflection. This is shown in the case of LDH + p-methylbenzoate intercalate. The figure 5.5 shows a situation when water molecules are arranged in the planes with COO^- groups coinciding with the LDH layers as one can see in the figure 3a in paper II. The figure 5.6 shows a situation when water molecules are freely distributed in a bulk between the LDH layers and the phenyl rings of the benzoate anions. The model describing this situation is shown in the figure 5.7 and the mentioned arrangement of interlayer water in this situation is not in agreement with experimental diffraction pattern.

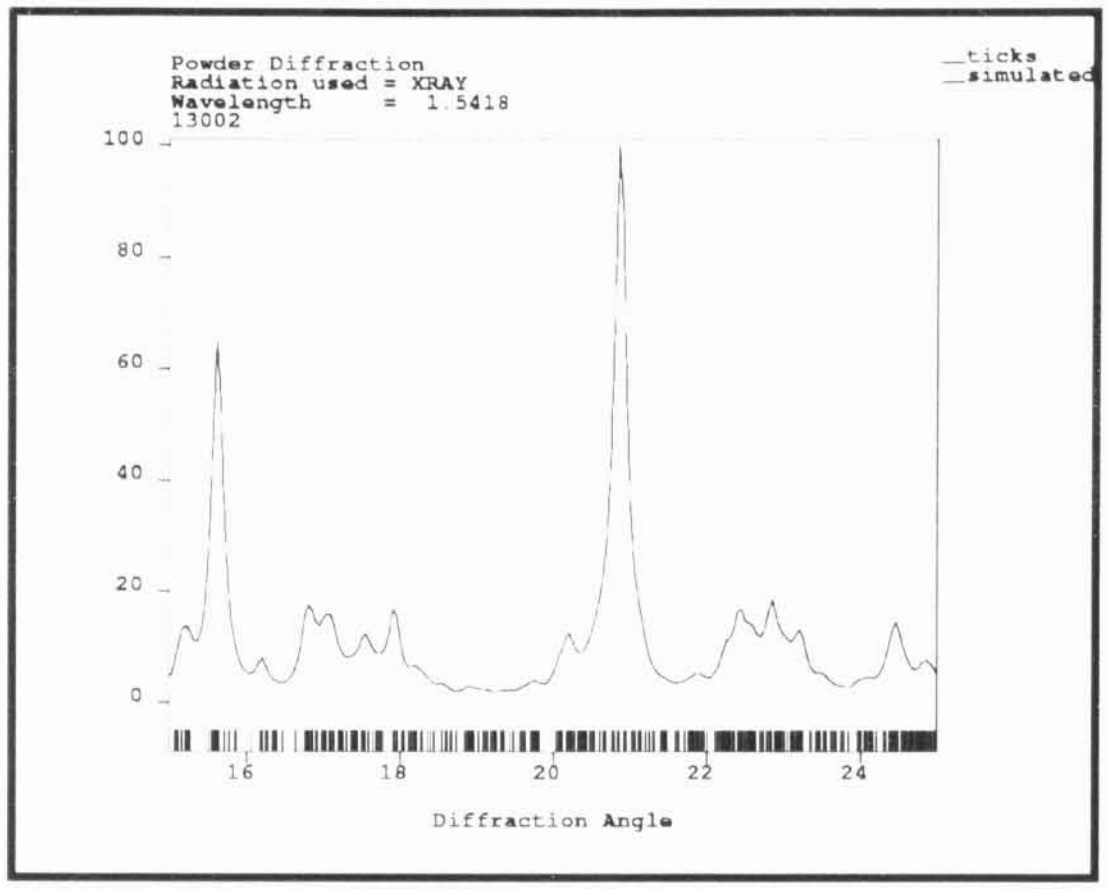

Fig. 5.5. A part of X-ray diffraction pattern of the LDH + p-methylbenzoate intercalate with an in-plane arrangement of water molecules. The (9 0 0) reflection corresponds to $2\theta = 15.7°$ and the (12 0 0) reflection to $2\theta = 21.0°$

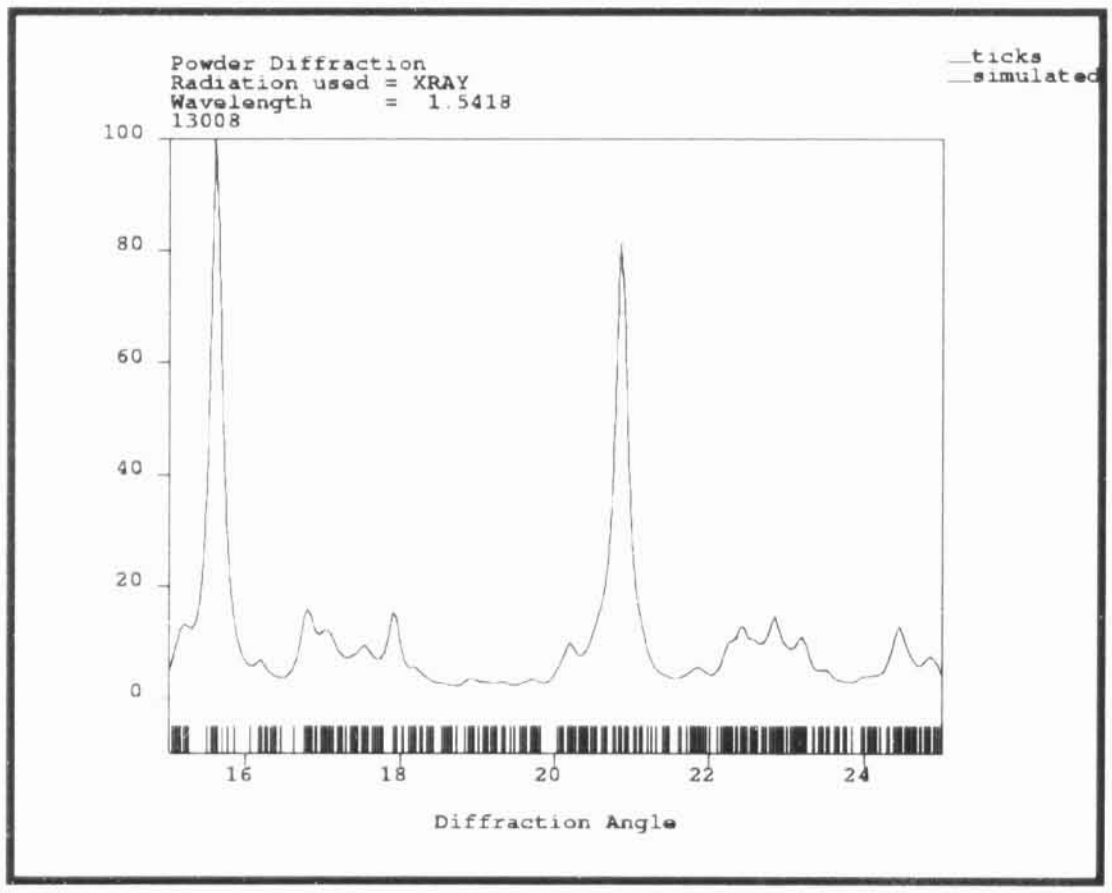

Fig. 5.6. A change of the intensity of (12 0 0) reflection corresponding to a „bulk“distribution of water molecules as it is shown in fig. 5.7.

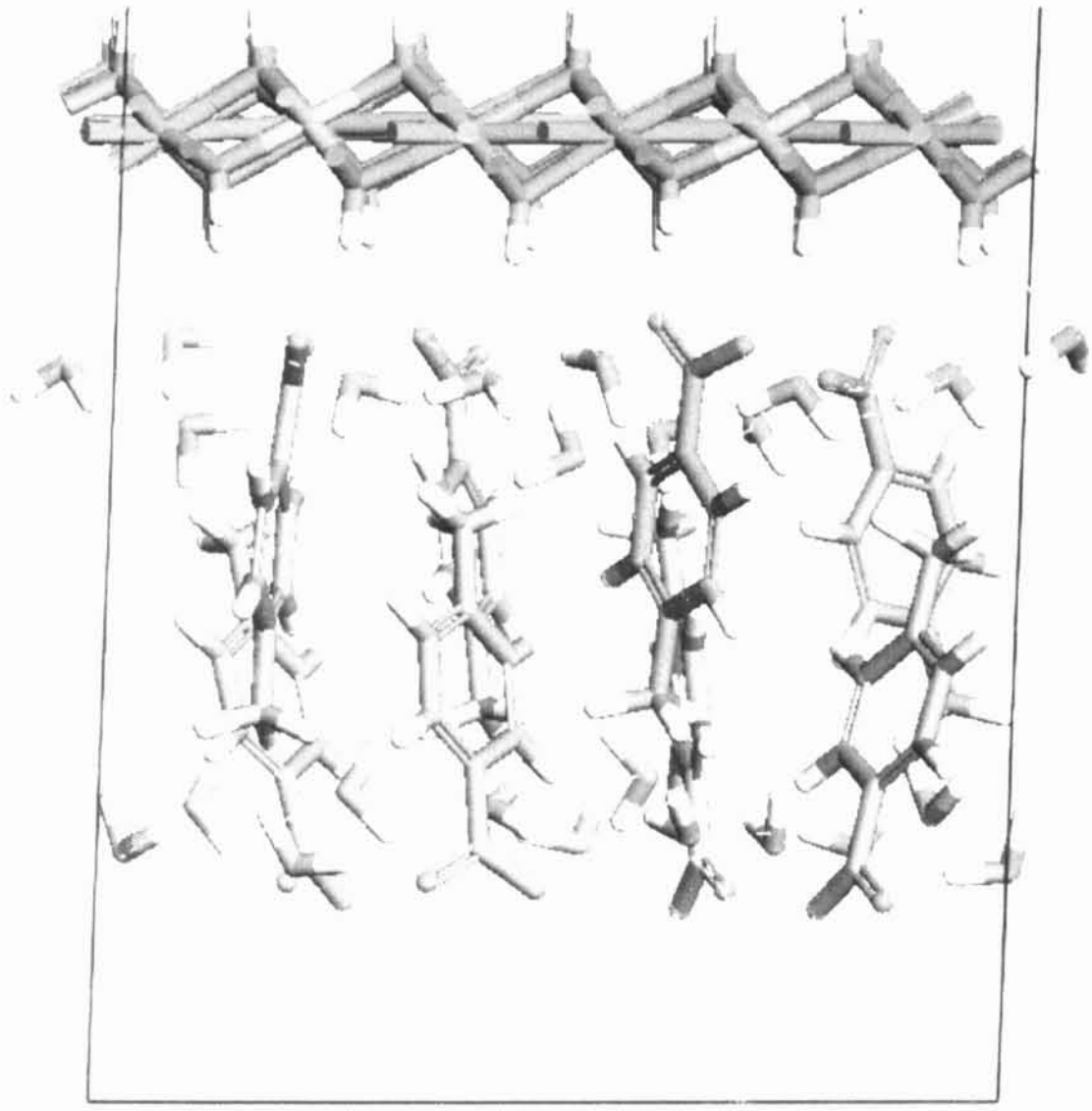

Fig. 5.7. A bulk distribution of water molecules between the LDH layers and the phenyl rings of the guests.

6. Conclusions

We worked out a molecular modeling strategy for solving structure of LDH intercalated with benzoate, p-methylbenzoate and p-bromobenzoate anions by methods of molecular simulations combined with X-ray diffraction.

In the case of LDH intercalated with benzoate the guests adopt as the best a parquet arrangement in the interlayer space. The addition of CH_3 groups and Br atoms in the p-positions of the benzoate ring cause a disorientation of the guests. CH_3 groups cause a „disordered rows arrangement" and the Br atoms lead to a total disorder of the guests in the interlayer space. The interlayer water molecules are located in the planes with COO^- groups near the LDH layers and location of interlayer water has a significant influence on the ratio of intensities of (9 0 0) and (12 0 0) diffraction peaks. If water molecules are freely distributed in a bulk the ratio of these two intensities changes with respect to the experimental diffraction pattern and it lead to a disagreement with the experimental diffraction pattern.

The energy minimization of structure models uses the so-called rigid units, where all the atoms in the layer keep their mutual distances and the layers themselves can move in a horizontal and in a vertical position. This molecular modeling strategy enables us to investigate the real influence of the arrangement of the interlayer region on the interlayer distance and enables us to investigate the stacking faults of the layers. In the case of using molecular dynamics calculations a quenched dynamics in a NVT statistical ensemble is suitable for conformational search. The modeling strategy that leads to the structure solving of smaller systems enables us to investigate much larger systems containing thousands of atoms. By using this strategy, we have solved structures of LDH intercalated with (5,10,15,20-tetrakis(4-sulfonatophenyl)porphyrin anions (TPPS anions) and LDH salt intercalated with ZnTPPS anions.

7. Acknowledgments

This work was supported by the Ministry of Education MSM 0021620835 and by the Grant Agency of the Czech Republic, grant no 203/05/2306

8. References:

[1] Sung-Ho Hwanga, Sang-Chul Jungb, Seon-Mi Yoonb, Dong-Kuk Kimb: (2008) *J. of Physics and Chemistry of Solids* 69:1061-1065

[2] Pigot T., Dupin J.C., Martinez H., Cantau C., Simon M., Lacombe S.: (2005) *Microporous and Mesoporous Materials* 84:343-352

[3] Lang K., Bezdička P., Bourdelande J.L., Hernando J., Jirka I., Káfuňková E., Kovanda F., Kubát P., Mosinger J. and Wagnerová D.M.: (2007) *Chem Mater* 19(15):3822-3829

[4] Laguna H., Loera S., Ibarra I.A., Lima E., Vera M.A., Lara V.: (2007) *Microporous and Mesoporous Materials* 98:234-241

[5] Feng Yang, Bo Yu Xie, Jing Zhi Sun, Jia Ke Jin, Mang Wang: (2008) *Materials Letters* 62:1302-1304

[6] Lei Lixu, Khan A., O'Hare D.: (2005) *J Solid State Chem* 178:3648-3654

[7] Tronto J., Leroux F., Crepaldi E.L., Naal Z., Klein S.I., Valim J.B.: (2006) *J Phys Chem Solids* 67:968-972

[8] Chen Aimin Xu, Hualong Hua et al.: (2005) *Top Catal* 35(1-2):177-185

[9] Newman S.P., Jones W.: (1999) *J Solid State Chem* 148(1):26-40

[10] Kooli F., Chisem I.C., Vucelic M. et al.: (1996) *Chem Mater* (8):1969-1977

[11] Vucelic M., Moggridge G.D.: (1995) *J Phys Chem* 99(20):8328-8337

[12] Moggridge G.D., Parent P., Tourilion G.: (1995) *Physica B* 209(1-4):269-270

[13] Moggridge G.D., Parent P., Tourillion G.: (1994) *Clays Clay Miner* 42(4):462-472

[14] Aimin Chen, Hualong Xu, Yinghong Yue, Weiming Hua, Wei Shen, Zi Gao: (2004) *Appl Catal A*: General 274:101–109

[15] Rives V.: *Layered double hydroxides present and future.* Nova Science Publishers, New York, (2001) pp 1–9

[16] Rives V., Ulibarri M.A.: (1999) *Coord Chem Rev* 181:61-120

[17] Rietveld H.M.: (1967) *Acta Cryst* 22:151

[18] Ling-Hao Su, Xiao-Gang Zhang, Chang-Huan Mi and Yan Liu: (2008) *J of Power Sources* (1)179:388-394

[19] Junwei Di, Jiongjia Cheng, Quan Xu, Huie Zheng, Jingyue Zhuang, Yongbo Sun, Keyu Wang, Xiangyin Mo and Shuping Bi: (2007) *Biosensors and Bioelectronics* 23:682-687

[20] Kovanda F., Jirátová K., Rymeš J., Koloušek D.: (2001) *Appl Clay Sci* 18:71-80

[21] Pacultová K., Obalová L., Kovanda F., Jirátová K.: (2008) Catalytic reduction of nitrous oxide with carbon monoxide over calcined Co–Mn–Al hydrotalcite *Catal Today; in press*

[22] Linares F.C., Solano S., Infante G.: (2004) *Microporous and Mesoporous Materials* 74:105-110

[23] Seo-Young Kwak, Yong-Joo Jeong, Jong-Sang Park, Jin-Ho Choy: (2002) *Solid State Ionics* 151:229-234

[24] Ulibarri M. Á., Del Carmen Hermosín M.: *Layered Double Hydroxides in water decontamination* in: V. Rives: *Layered double hydroxides present and future*. Nova Science Publishers, New York, (2001) pp 285-321

[25] Giacovazo C.: *Fundamentals of Crystallography*. Oxford University Press Inc., New York, 1992

[26] Snyder R.L., Fiala J., Bunge H.J.: *Defect and microstructure analysis by diffraction*. Oxford University Press Inc., New York, 1999

[27] *Cerius² User Guide*, Month 1997. San Diego: Molecular Simulations Inc., 1997.

[28] Comba P., Hambley T.W.: *Molecular modeling of inorganic compounds*. VCH, Weinheim, (1995)

[29] Rappé A.K., Goddard W.A.: (1991) *J Phys Chem* 95:3358-3363

[30] Karasawa N., Goddard W.A.: (1989) *J Phys Chem* 93:7320-7327

[31] V. Rives: *Layered double hydroxides present and future*. Nova Science Publishers, New York, (2001) pp 105

[32] Rappe A.K., Casewit C.J., Colwell K.S., Goddard III W.A., Skiff W.M.: (1992) *J Am Chem Soc* 114 10024-10035

9. Publications

I. Petr Kovář, Miroslav Pospíšil, Morena Nocchetti, Pavla Čapková and Klára Melánová: Molecular modeling of layered double hydroxide intercalated with benzoate, modeling and experiment. *Journal of Molecular Modeling (2007) 13:937–942*

II. Petr Kovář, Klára Melánová, Vítězslav Zima, Ludvík Beneš and Pavla Čapková: Layered double hydroxide intercalated with *p*-methylbenzoate and *p*-bromobenzoate: Molecular simulations and XRD analysis. *Journal of Colloid and Interface Science (2008) 319: 19–24*

I.
Molecular modeling of layered double hydroxide intercalated with benzoate. modeling and experiment

J Mol Model (2007) 13:937–942
DOI 10.1007/s00894-007-0217-4

ORIGINAL PAPER

Molecular modeling of layered double hydroxide intercalated with benzoate, modeling and experiment

Petr Kovář · M. Pospíšil · M. Nocchetti · P. Čapková · Klára Melánova

Received: 1 March 2007 / Accepted: 14 May 2007 / Published online: 9 June 2007

Abstract The structure of Zn_2Al Layered Double Hydroxide intercalated with benzenecarboxylate ($C_6H_5COO^-$) was solved using molecular modeling combined with experiment (X-ray powder diffraction, IR spectroscopy, TG measurements). Molecular modeling revealed the arrangement of guest molecules, layer stacking, water content and water location in the interlayer space of the host structure. Molecular modeling using empirical force field was carried out in Cerius^2 modeling environment. Results of modeling were confronted with experiment that means comparing the calculated and measured diffraction pattern and comparing the calculated water content with the thermogravimetric value. Good agreement has been achieved between calculated and measured basal spacing: $d_{(00l)}$=15.3 Å and $d_{(00l)}$=15.5 Å. The number of water molecules per formula unit (6H$_2$O per $Zn_2Al_2(OH)_{12}$) obtained by modeling (i.e., corresponding to the energy minimum) agrees with the water content estimated by thermogravimetry. The long axis of guest molecules are almost perpendicular to the LDH layers, anchored to the host layers via COO^- groups. Mutual orientation of benzoate ring planes in the interlayer space keeps the parquet arrangement. Water molecules are roughly arranged in planes adjacent to host layers together with COO^- groups.

Keywords Benzoate · Layered double hydroxide · Molecular modeling · X-ray diffraction

P. Kovář (✉) · M. Pospíšil · P. Čapková
Faculty of Mathematics and Physics, Charles University Prague,
Ke Karlovu 3,
12116 Prague 2, Czech Republic
e-mail: kovar@karlov.mff.cuni.cz

M. Nocchetti
Centro di Eccellenza Materiali Innovativi Nanostrutturati,
Dipartimento di Chimica, Universita di Perugia,
Via Elce di Sotto, 8,
06123 Perugia, Italy

K. Melánova
Joint Laboratory of Solid State Chemistry,
University of Pardubice,
Studentska 84,
53210 Pardubice, Czech Republic

P. Čapková
Institute of Materials Chemistry, Technical University Ostrava,
17 listopadu 15,
70833 Ostrava - Poruba, Czech Republic

Introduction

Layered double hydroxides (LDHs), sometimes called hydrotalcites, belong to a wide family of lamellar compounds called anionic clays. They are characterized by regular stacking of layers that bear a positive charge. The layers are formed of octahedral units $M(OH)_2$ where M is mostly a divalent or a trivalent cation. The interlayer space contains water molecules and anions that compensate the positive charge of the layers. Hydrotalcites can be represented by a general formula:

$$\left[M^{2+}_{1-x}M^{3+}_{x}(OH)_2\right]^{x+}\left[A^{n-}_{x/n}\right]^{-} \cdot m\ H_2O,$$

where M^{2+} and M^{3+} are bi- and trivalent metal cations, A is the interlayer anion with the charge of n^- [1].

The charge balancing anions can be exchanged by a wide amount of anions of inorganic or organic molecules [1–4]. The anion exchange is a widely used intercalation method [5, 6].

LDH offer a wide scale of practical application like catalysts (e.g., precursors for preparation of other catalysts [7], synthesis of organic molecules [8], chemical reactions [9]), polymer stabilizers [10, 11], drug carriers [12] and drug improvers [13], sorbents [14, 15], etc. Intercalation of guest species possessing chromophoric groups into LDH gives rise to hybrid organo - inorganic nanostructure materials for various photofunction [16, 17].

In the present work we investigated the structure of LDH intercalated with benzoate anions. Many papers dealing with LDH intercalated with benzoic acid and its derivatives such as salts of benzoic acid, terephthalate have been published [18–25] mostly with only on a rough assessment of structure model based on the measured basal spacing. In this paper we investigated the structure and guest arrangement in benzoate - LDH intercalate using combination of molecular modeling with experiment (X-ray powder diffraction, IR spectroscopy and thermogravimetry).

Experiment

Samples preparation and chemical analysis

Well crystallized hydrotalcite - like compound (HTlc) of formula $[Zn_4Al_2(OH)_{12}](CO_3)\cdot 2,4H_2O$, was obtained with a procedure accomplished by the thermal hydrolysis of urea [26]. The corresponding chloride form was obtained by titrating the carbonate form, dispersed in a 0.1 mol·dm^{-3} NaCl solution, with a 0.1 mol·dm^{-3} HCl by means of Radiometer automatic titrator operating at pH stat mode, and pH value of 5. Finally, the hydrotalcite in nitrate form was obtained by equilibrating the chloride form with an aqueous solution of $NaNO_3$ 0.5 mol·dm^{-3} (molar ratio $NO_3^-/Cl^- = 10$). The composition of host structure was the following:

$$[Zn_4Al_2(OH)_{12}](NO_3)_2\cdot 4,5\ H_2O$$

The intercalation of benzoate anions was achieved by equilibrating the nitrate form of hydrotalcite with an aqueous solution of C_6H_5COONa 0.5 mol·dm^{-3} (molar ratio $C_6H_5COO^-_{solution}/NO_{3\,solid}^- = 10$) for 24 hours. The recovered solid was three times washed with CO_2-free deionized water and dried over P_4O_{10}. The composition of the intercalated structure was:

$$[Zn_4Al_2(OH)_{12}](C_6H_5COO)_2\cdot 6\ H_2O$$

The Zn and Al content of the HTlc, was obtained with standard EDTA titration after having dissolved a weighed amount of the sample (~100 mg) in a few drops of concentrated HCl and diluted with water to 50 ml. The Cl^-, NO_3^- and $C_6H_5COO^-$ counterions in solution, before and after equilibration, were determined by ion chromatography. Water and $C_6H_5COO^-$ content of the solids were obtained by thermogravimetry.

TG DTA analysis were performed in air by a Stanton 781 Thermoanalyser at the heating rate of 5 °C/min.

The thermogravimetric analysis (TGA) and differential thermal analysis (DTA) showed two endothermic peaks related to loss of co-intercalated water and to dehydroxylation of the inorganic layers between 80 °C and 300 °C. Furthermore, the main weight loss between 300 °C and 600 °C may be ascribed to decomposition of organic parts. ZnO and $ZnAl_2O_4$, starts to be formed at temperatures higher than 600 °C as confirmed by the XRPD patterns of the sample heated at 900 °C.

X-ray diffraction

The measurement conditions: X-ray powder diffraction (XRPD) patterns were taken with a computer-controlled PW 1710 Philips diffractometer operating at 40 kV, 30 mA, using a PW 1820 gonometer, supplied with a bent graphite monochromator in the diffracted beam, and Cu-Kα radiation. XRPD patterns were taken with the step-scanning technique. The samples were prepared using the side-loading procedure in order to minimize preferred orientations. Diffractograms were collected from $2\theta°=2$ to 120° using steps of 0.01° and a counting time of 20 s per step.

The diffraction pattern of the intercalated structure measured at temperature of 30 °C is shown in Fig. 1. It exhibits characteristic features of a layered structure, that means very strong basal reflections due to the strong preferred orientation and weak broaden non-basal reflections indicating a slight stacking disorder. Nevertheless the crystal structure of the intercalate exhibits a high degree of three-dimensional ordering (non-basal reflections quite pronounced). Anyway due to the slight structural disorder

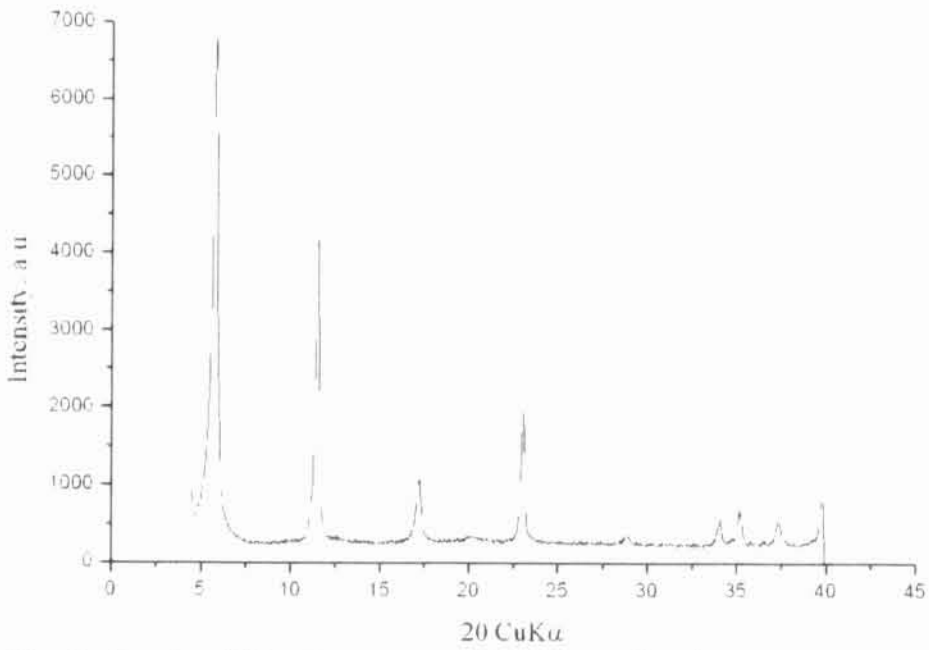

Fig. 1 Powder diffraction pattern of the intercalated structure

the structure of the intercalate cannot be solved by diffraction method only and it is suitable to use molecular modeling.

IR spectroscopy

FT-IR spectra of the solid samples were recorded under vacuum with a Bruker IFS 113V spectrometer by the KBr pellet technique.

The FT-IR spectrum (see Fig. 2) shows a strong broad band in the 3000–3750 cm^{-1} range due to the lamellae OH stretching which are involved in H- bonds. The sharp and intense bands at 1537 cm^{-1} and 1397 cm^{-1} are ascribable to the asymmetric and symmetric stretching vibrations of the equivalent carbon-oxygen bonds of COO^- group. Moreover, are visible the typical signals of monosubstituted aromatic ring: the in-plane skeletal vibration at 1595 cm^{-1} and the two adsorption bands at 719 cm^{-1} and 689 cm^{-1} due to the bending of the five adjacent hydrogen atoms of the ring.

Molecular modeling

Molecular modeling using an empirical force field was carried out in *Cerius*^{2} modeling environment [27]. Initial model of the host structure was built according the crystallographic structure data obtained from refinement by means of Rietveld procedure. Unit cell of the host structure is trilayer, the space group is *R-3m* with trielinic cell and lattice parameters $a = 3.07598$ Å, $c = 23.2048$ Å, $\alpha = 90°$, $\beta = 90°$, $\gamma = 120°$.

The Al and Zn atoms in the host layers were randomly distributed so that the composition of the host structure corresponded to the experimental one. The measured value of basal spacing, was $d_{(0,0,3)} = 15.5$ Å, thus the interlayer distance in the initial model was set to this value. To investigate the arrangement of guest molecules in the interlayer space we built the supercell $4a \times 6a \times 1c$ with the lattice parameters: $4a = 12.3039$ Å, $6a = 18.4559$ Å, where the $c = 3d_{(0,0,3)} = 46.5$ Å. The charge of this trilayer supercell is $+24$ el_-, that means 24 benzoate anions were placed into the interlayer space of the supercell, consisting of 3 host layers and 3 guest layers (i.e., 8 benzoates per one guest layer in the supercell).

A series of initial models have been built with various positions and orientations of guests and with variable water content:

(1) Benzoate ring planes parallel to the host layers in bilayer or trilayer guest arrangement in the interlayer space.
(2) Benzoate ring planes tilted to the host layers in bilayer guest arrangement in the interlayer space.
(3) Benzoate ring planes perpendicular to the host layers and with various mutual orientations and various positions of COO^- groups with respect to OH groups on the host structure.

Energy minimization was carried out in *Universal force field* [28]. The electrostatic energy was calculated by Ewald summation method [29], van der Waals energy was expressed by Lennard-Jones potential [30]. The minimization of the total crystal energy was carried out in the *Minimizer* module according to the following strategy:

All the host layers in the supercell were kept as rigid units during energy minimization. Variable parameters were: c, α, β (this enables to optimize the mutual positions of the layers) and all atomic positions in guest layers. The minimization was carried out by modified Newton procedure.

The calculated structure models obtained from various starting geometries were sorted using two criteria:

The value of crystal energy minimum.
The similarity of calculated and measured diffraction pattern.

After reaching the optimum positions and orientation of guest molecules we tried to find the optimum water content and water location. As the water content has the significant influence on the total energy we could find the optimum water content. The following strategy was used: We compared the total nonbonded energy (i.e., sum of electrostatic and van der Waals interactions) of the optimized structure models containing various water content in the interlayer space. By using this procedure we can find out the affinity rate of water molecules to the interlayer space. On the other hand position of water molecules in the interlayer space affects strongly the intensity profiles in the diffraction pattern. This effect enables us to refine the water location.

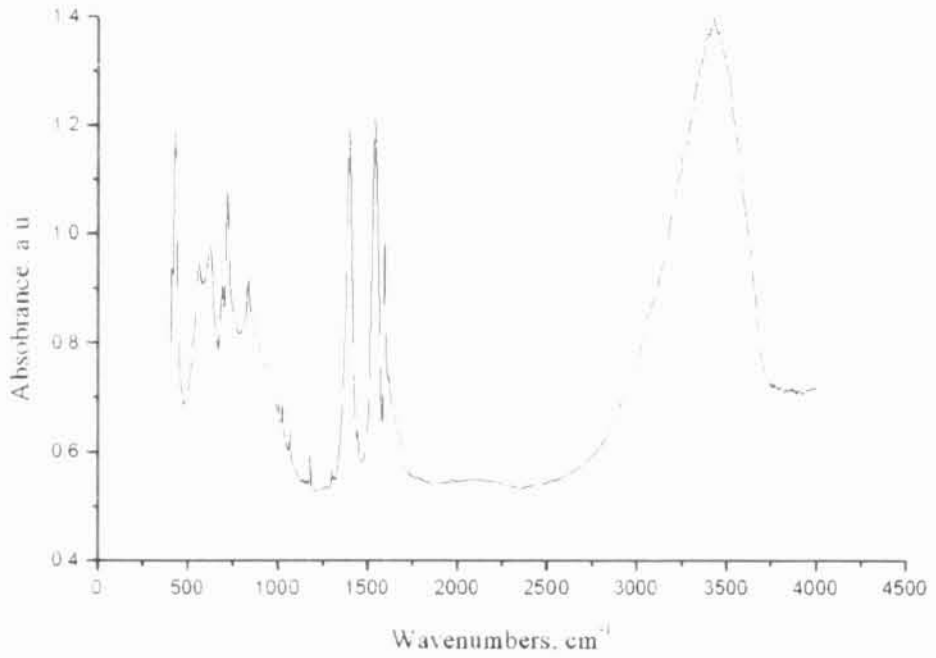

Fig. 2 IR spectra of the intercalated structure

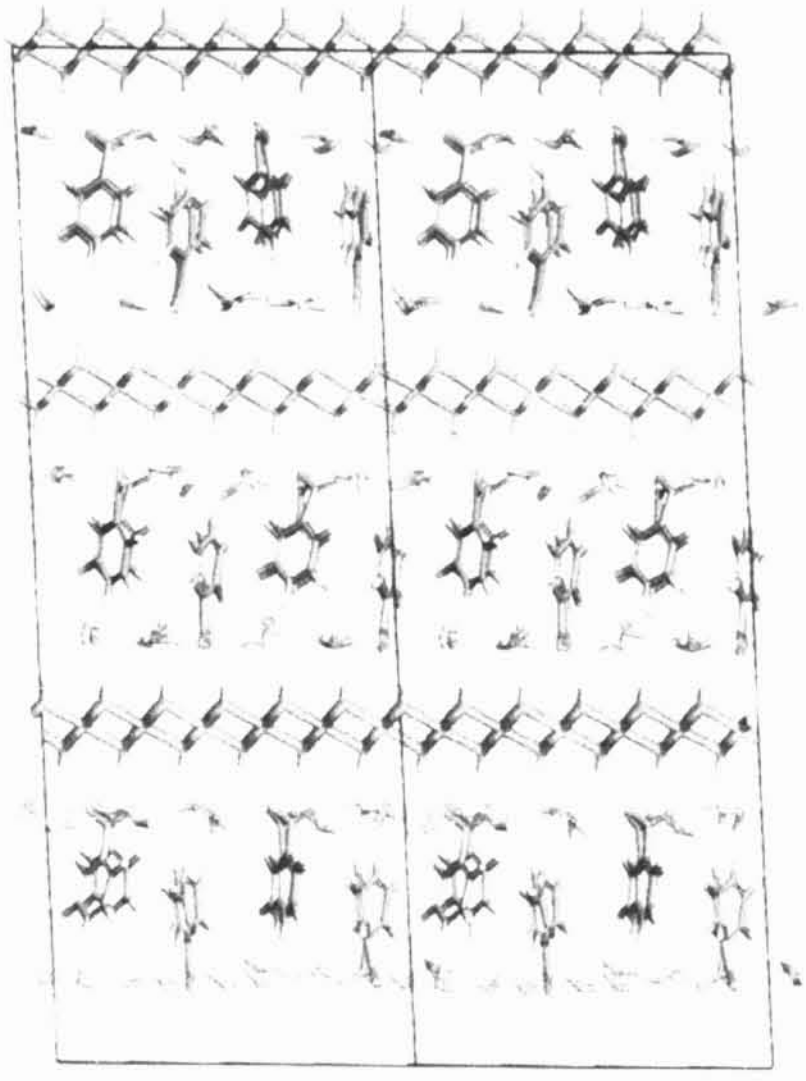

Fig. 3 Side view of the optimized structure with the hydrogen-bond interactions (broken line)

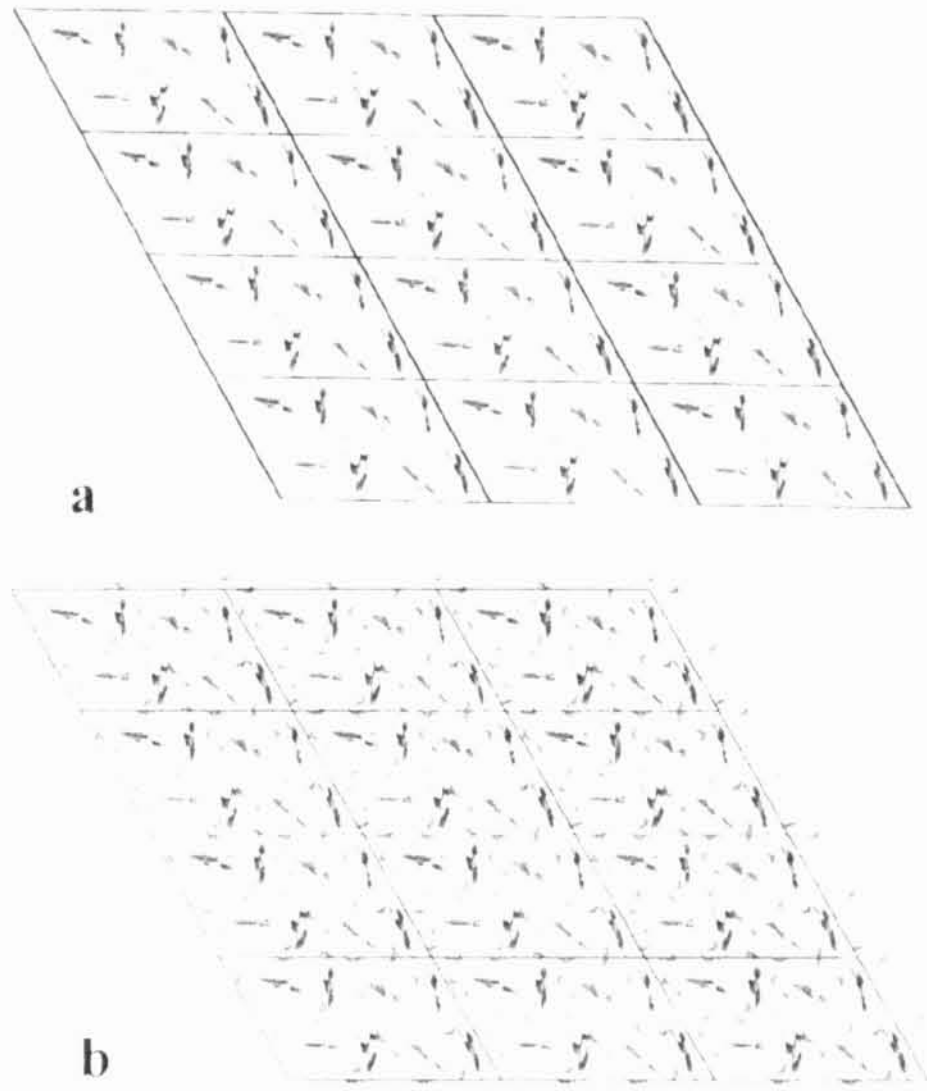

Fig. 5 a) Top view of parquet arrangement of the ring planes **b)** Top view of parquet arrangement of the ring planes and arrangement of water molecules

Results

Results of modeling led to the conclusions concerning the orientation and position of the benzoate anions in the interlayer space. The optimized structure model is shown in Fig. 3. The long axis of benzoate is oriented perpendicular to the hydrotalcite layers with small departure within the range of ±10 degrees. COO^- groups are anchored to OH groups of the LDH layer via the hydrogen bond. The detailed view of orientation of COO^- groups with respect to OH groups is shown in Fig. 4. Carboxyl group can rotate freely along the C-C bond in long benzoate axis that means while the ring planes exhibit ordering, the orientation of carboxyl groups is disordered. Mutual orientation of the ring planes keeps parquet arrangement with a small departure within the range of ±10 degrees (see Fig. 5a,b).

Mutual positions of two successive host layers in the intercalated structure exhibit a slight shift from their starting

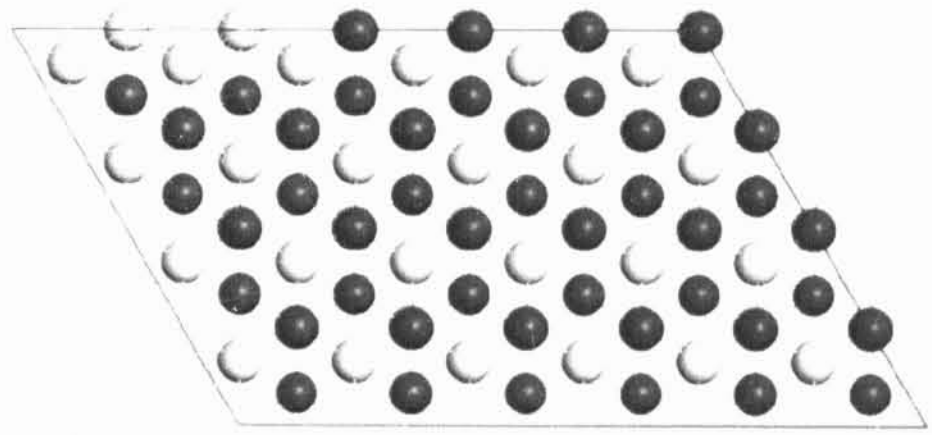

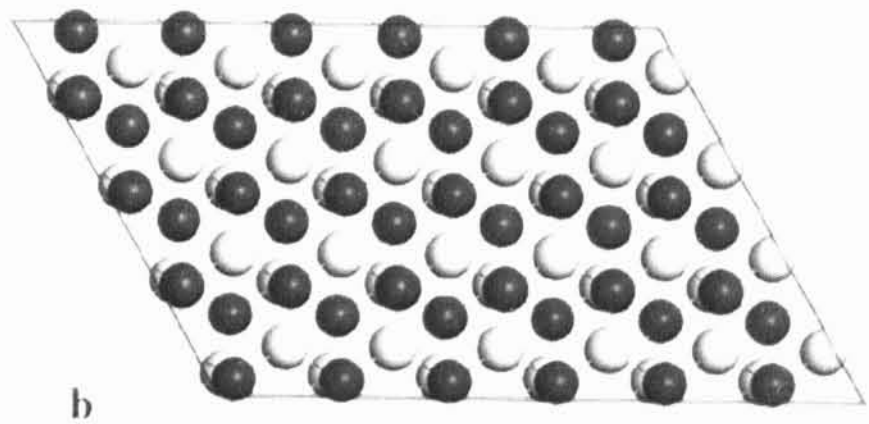

Fig. 6 a) Top view of stacking of two successive layers in the starting model (metal atoms represented by bright balls, oxygen atoms represented by dark balls) **b)** Top view of stacking of two successive layers in the optimized model (metal atoms represented by bright balls, oxygen atoms represented by dark balls)

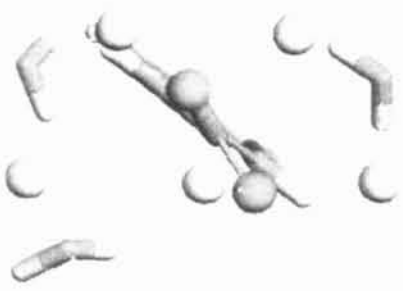

Fig. 4 Detailed top view of the orientation of COO^- groups with respect to the OH groups (gray balls represent hydrogen atoms of OH groups of the layer)

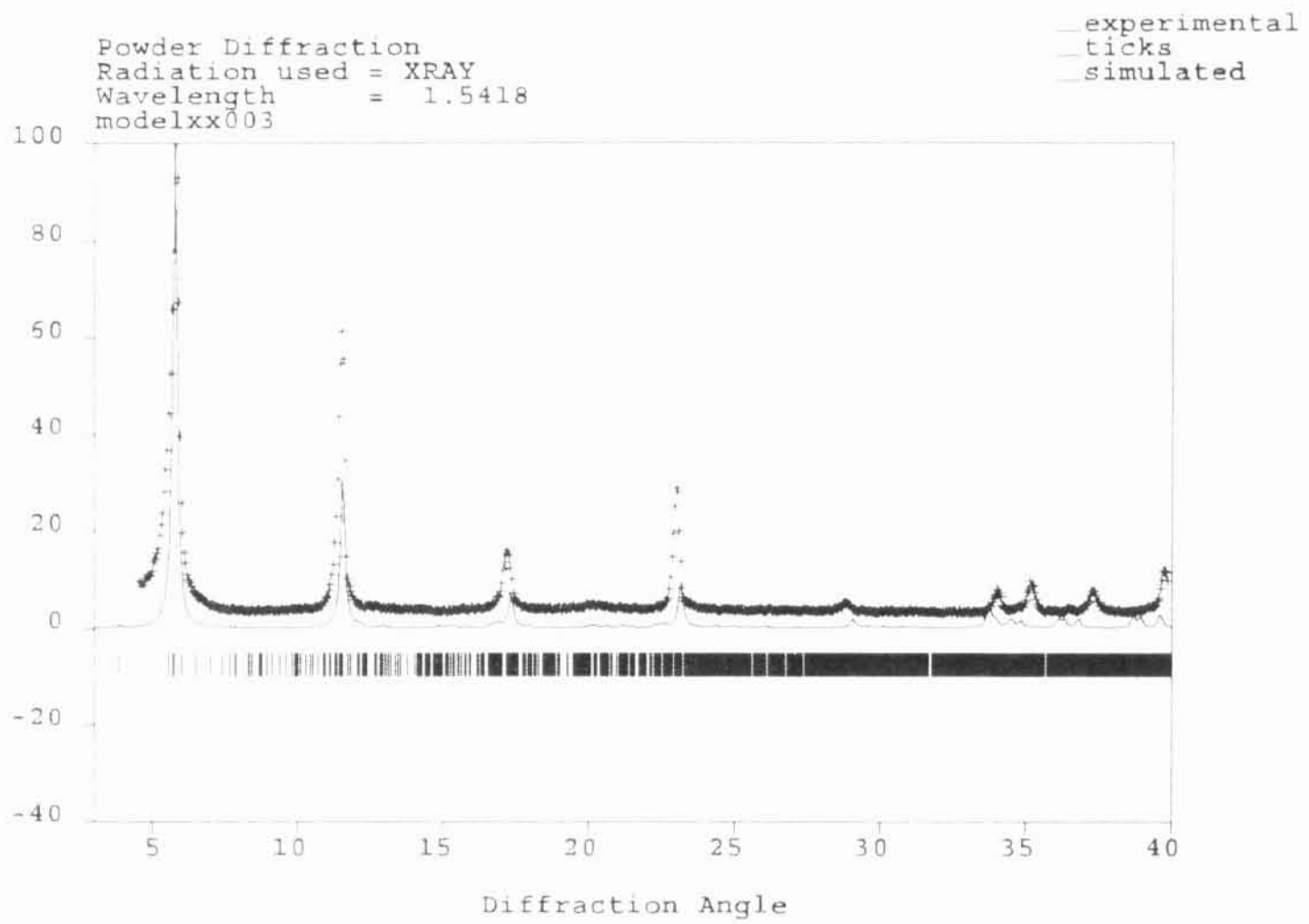

Fig. 7 Calculated powder diffraction pattern

positions in the host structure. This shift in direction along metal - oxygen bonds is about 0.3 Å at maximum (see Fig. 6a,b).

The calculated diffraction pattern of the optimized structure is shown in Fig. 7. The higher intensity of basal reflection with respect to the others in comparison to the experimental diffraction pattern is due to the roughness of the surface of the experimental sample which is not taken into account in the calculating software. The roughness of the surface takes effect just at low values of diffraction angle and results in a decline of the intensity of basal reflection in the experimental diffraction pattern. Optimum water content found using energy minimization is 72 water molecules per unit cell, that means 24 H_2O in one guest layer, see Table 1. This water content is in good agreement with that estimated by thermogravimetric measurement. The location of water molecules refined using comparison of calculated and measured intensity ratio in the diffraction pattern is illustrated in Figs. 5 and 5b. Water molecules are not regularly distributed in the interlayer space, but concentrated in the two planes adjacent to the host layers coinciding with the COO^- planes, as they are hydrogen bonded to the OH groups in host layers and to carboxyl groups.

Discussion and conclusions

Molecular modeling enabled us to solve the crystal structure of benzenecarboxylate-LDH intercalate, where the conventional diffraction analysis failed due to the slight structural disorder, caused by the slight disorientation of guests.

Molecular modeling provides not only the detailed structure model but in addition revealed the character of this disorder. There is a slight disorder arising from mutual slight shift of two successive host layers. This disorder in the host layers is a consequence of slight disorder in the orientation of guests (rotation about long guest axis), disorder in orientation of carboxyl groups and in position of guests on the host layers. Results of the present work show that molecular modeling is useful not only in

Table 1 Comparing the total nonbonded energy of models containing various number n of water molecules per one interlayer space

n	Γ_{total} kcal	Γ_{elst} kcal	Γ_{vdW} kcal	d_{calc} Å
20	−15051	−14830	−221	15.2
22	−15165	−14977	−188	15.2
24	−15363	−15167	−196	15.3
26	−15200	−15110	−90	15.3
28	−15110	−15050	−60	15.4

structure analysis but also in estimation of water content and guest concentration. The close cooperation of modeling and experiment is a necessary requirement for successful structure solution.

Acknowledgments This work was supported by the Grant Agency of the Czech Republic, grant no 203/05/2306, and by the Ministry of Education MSM 0021620835 and MSM 6198910016.

References

1. Rives V (2001) Layered double hydroxides present and future. Nova Science Publishers, New York, pp 1–38
2. Steven P, Jones W, Jones N (1998) New J Chem 22:105–115
3. Zhang X, Wei M (2005) J Sol State Chem 178:2701–2708
4. Aloisi G, Stammirova T, Hibino T (2006) Appl Clay Sci 31:65–75
5. Ishikawa T, Matsumoto K, Kandori K, Nakayama T (2007) Colloids Surfaces A 293:135–145
6. Radha AV, Kamath PV, Shivakumara C (2005) Solid State Sci 7:1180–1187
7. Turco M, Bagnasco G, Costantino U, Marmottini F, Montanari T, Ramis G, Busca G (2004) J Catal 228:43–55
8. Vaccari A (1999) Appl Clay Sci 14:161–198
9. Greenwell HC, Holliman PJ, Jones W, Velasco BV (2006) Catal Today 114:397–402
10. Liu Y, Wang L, Evans DG, Li D (2006) J Phys Chem Solids 67:998–1001
11. Van der Ven L, Van Gemert MLM, Batenburg LF, Keern JJ, Gielgens LH, Koster THM, Fischer HR (2000) Appl Clay Sci 17:25–34
12. Costantino U, Nocchetti M, Layered Double Hydroxides and their intercalation compounds in Photochemistry and Medicinal Chemistry Chapter 8. In: Ref. Rives V (2001) Layered double hydroxides Present and future. Nova Science Publishers, New York, pp 435–468
13. Ambrogi V, Fardella G, Grandolini G et al (2003) J Pharm Sci 92 (7):1407–1418
14. Orthman J, Zhu HY, Lu GQ (2003) Separation Purification Technol 31:53–59
15. De Jong KP (2006) J Phys Chem B 110:9211–9218
16. Latterini L, Nocchetti M, Aloisi GG, Costantino U, Elisei F (2007) Inorg Chim Acta 360:728–740
17. Ogawa M, Kuroda K (1995) Chem Rev 339:335–341
18. Lei L, Khan A, O'Hare D (2005) J Solid State Chem 178:3648–3654
19. Tronto J, Leroux F, Crepaldi EL, Naal Z, Klein SI, Valim JB (2006) J Phys Chem Solids 67:968–972
20. Chen YM, Xu HL, Hua WM et al (2005) Top Catal 35(1–2):177–185
21. Newman SP, Jones W (1999) J Solid State Chem 148(1):26–40
22. Kooli F, Chisem IC, Vucelic M et al (1996) Chem Mater 8 (8):1969–1977
23. Vucelic M, Moggridge GD (1995) J Phys Chem 99(20):8328–8337
24. Moggridge GD, Parent P, Tourillon G (1995) Physica B 209(1–4):269–270
25. Moggridge GD, Parent P, Tourillion G (1994) Clays Clay Miner 42(4):462–472
26. Costantino U, Marmottini F, Nocchetti M, Vivani R (1998) Eur J Inorg Chem 1998:1439–1446
27. Comba P, Hambley TW (1995) Molecular Modeling of Inorganic Compounds VCH Verlagsgesselschaft mbH, Weinheim, pp 28–31
28. Rappe AK, Casewit CJ, Colwell KS, Goddard III WA, Skiff WM (1992) J Am Chem Soc 114:10024–10035
29. Karasawa N, Goddard WA (1989) J Phys Chem 93:7320–7327
30. Lennard-Jones JE (1925) Proc Royal Society of London, series A 109(752):584–597

II.
Layered double hydroxide intercalated with *p*-methylbenzoate and *p*-bromobenzoate: Molecular simulations and XRD analysis

Available online at www.sciencedirect.com

ScienceDirect

Journal of Colloid and Interface Science 319 (2008) 19–24

JOURNAL OF
Colloid and
Interface Science

www.elsevier.com/locate/jcis

Layered double hydroxide intercalated with *p*-methylbenzoate and *p*-bromobenzoate: Molecular simulations and XRD analysis

Petr Kovář [a,*], Klára Melánová [b], Vítězslav Zima [b], Ludvík Beneš [b], Pavla Čapková [c]

[a] *Faculty of Mathematics and Physics, Charles University Prague, Ke Karlovu 3, 12116 Prague 2, Czech Republic*

[b] *Joint Laboratory of Solid State Chemistry of Institute of Macromolecular Chemistry of Academy of Sciences and University of Pardubice (Faculty of Chemical Technology), Studentská 84, 532 10 Pardubice, Czech Republic*

[c] *Nanotechnology Centre, Technical University Ostrava, 17. Listopadu 15, 70833 Ostrava, Czech Republic*

Received 21 July 2007; accepted 25 October 2007

Available online 11 December 2007

Abstract

Samples of Mg_4Al_2 layered double hydroxide (LDH) intercalated with *p*-methylbenzoate and *p*-bromobenzoate anions were prepared by reconstruction of calcined LDH. The interlayer arrangement of guests was investigated by molecular modeling combined with X-ray powder diffraction and thermogravimetry. Molecular modeling was carried out in a Cerius^2 modeling environment. In both structures the guest anions adopt a nearly perpendicular arrangement of their long axis with respect to the host layers and they are anchored to the OH groups of the layers through COO^- groups via electrostatic interactions. Molecular modeling revealed that both structures of the intercalates exhibit a certain disorder of guest anions in the interlayer space. In the case of LDH–*p*-methylbenzoate intercalate the anions tend to be situated in disordered rows, and the LDH–*p*-bromobenzoate intercalate exhibits a total disorientation of guest anions. A good agreement between calculated and measured X-ray diffraction patterns and between experimental and calculated basal spacings was obtained. In the LDH–*p*-methylbenzoate intercalate $d_{exp} = 16.96$ Å and $d_{calc} = 16.97$ Å, and in the case of LDH–*p*-bromobenzoate intercalate $d_{exp} = 17.19$ Å and $d_{calc} = 17.40$ Å.

Keywords: Layered double hydroxide; *p*-Bromobenzoate; *p*-Methylbenzoate; Molecular simulations; X-ray diffraction

1. Introduction

Layered double hydroxides (LDH) consist of positively charged brucite-like layers and negatively charged anions in the interlayer space. These structures can be represented by the following general formula

$$\left[M^{2+}_{1-x}M^{3+}_{x}(OH)_2\right]^{x+}\left[\left(A^{n-}\right)_{x/n}\cdot mH_2O\right],$$

where M^{2+} and M^{3+} are di- and trivalent metal cations, respectively, A^{n-} represents an exchangeable interlayer anion with the charge of n^- [1]. LDH systems were widely studied for advancing their potential applications and from a molecular simulations point of view, e.g., Hou, Kirkpatrick, and coworkers [2,3].

Since there is a high versatility of organic and inorganic anions that can possibly be exchanged for the A^{n-} anions, the intercalated layered double hydroxides are the object of special interest due to the possibility of a wide practical use in many industrial and scientific fields such as medicinal chemistry [4], catalysis [5,6], and ecology [7]. Intercalation of guest species possessing chromophoric groups into LDH gives rise to hybrid organo-inorganic nanostructure materials for various photofunctions [8,9]. Investigation of the interlayer arrangement of these compounds is in general difficult as they usually exhibit a certain degree of disorder, which can obstruct the structure analysis based on diffraction data only. A method that successfully solves this problem is a combination of molecular modeling and experimental measurements. As a result we can obtain a detailed structure model including a characterization of possible disorder, the energy characteristics, e.g., the total sublimation energy and its van der Waals and electrostatic contributions.

* Corresponding author.
E-mail address: kovar@karlov.mff.cuni.cz (P. Kovář).

0021-9797/$ – see front matter
doi:10.1016/j.jcis.2007.10.060

Since the chemical, optical, and other properties of the intercalates are influenced by the structure of the interlayer space, molecular modeling can reveal the relationship between the structure and the properties of the investigated material.

An extensive work dealing with geometric isomers of benzoate derivatives was done from an experimental point of view [10]. In this work we simulated the arrangement of the interlayer space of LDH–*p*-methylbenzoate and LDH–*p*-bromobenzoate intercalates. The arrangement was investigated by a combination of molecular modeling, X-ray diffraction, and thermogravimetry.

2. Experimental

A large amount of Mg–Al–CO_3 hydrotalcite, with the formula $[Mg_{0.67}Al_{0.33}(OH)_2](CO_3)_{0.165}\cdot 0.5H_2O$, was prepared by a urea method [11]. A solution obtained by mixing 100 mL of 0.5 M $AlCl_3$, 200 mL of 0.5 M $MgCl_2$, and 30 g of urea was refluxed for 2 days. The precipitate obtained was filtered, washed with distilled water, and equilibrated with 100 mL of 0.1 M Na_2CO_3 for 1 day. Then the solid was recovered by filtration, washed with distilled water, and dried in air.

Mg–Al–CO_3 (0.234 g) was calcined at 400 °C for 3 h. The calcined powders were added into a solution of 1.5 mmol of corresponding acid (6.41 mmol of acid per gram of Mg–Al–CO_3) in 9 ml of CO_2-free water and hydrothermally treated at 130 °C for 60 h. The intercalates prepared were filtered, washed with CO_2-free distilled water, and dried. The contents of magnesium, aluminum, and bromine were determined by an energy-dispersive X-ray spectrometry (EDX) microanalysis. The content of the guest anions was determined by elemental analysis (C, H) and the water content was calculated from thermogravimetry. The formulas of the intercalates prepared and the amounts of acids used for the synthesis are given in Table 1 together with the results of TGA and elemental analyses.

Powder X-ray diffraction data were obtained with a D8-advance diffractometer (Bruker AXS, Germany) using Cu$K\alpha$ radiation with a secondary graphite monochromator. Diffraction angles were measured from 2° to 70° (2θ).

The TGA were done using a homemade apparatus constructed of a computer-controlled oven and a Sartorius BP210 S balance. The measurements were carried out in air between 30 and 900 °C at a heating rate of 5 °C min^{-1}.

3. Molecular modeling

Molecular modeling using an empirical force field was carried out in Cerius^2 modeling environment [12]. The first stage in preparing models of the intercalates was construction of the host framework. It was constructed according to the reported structure data in [1]. The host structure is trilayered and it consists of a rombohedral lattice with hexagonal unit-cell parameters $a = 3.054$ Å, $c = 22.81$ Å, and space group is $R3$-m. The Mg and Al atoms were randomly distributed in every layer so that the ratio of the amount of Mg and Al atoms in the host framework was 2:1. To investigate the mutual arrangement of the guests in the interlayer space we created a $P1$ superlattice with the dimensions $6a \times 4a \times 3d_{exp}$, where d_{exp} was taken over from the X-ray diffraction data. In the case of LDH–*p*-bromobenzoate intercalate $d_{exp} = 17.19$ Å and in the case of LDH–*p*-methylbenzoate intercalate $d_{exp} = 16.96$ Å.

The charge of this trilayered superlattice was +24 el., i.e., +8 el. per each host layer. The positive layer charge was compensated by 8 guest anions that were inserted into the interlayer space. The amount of water (24 molecules per one interlayer space) was taken over from the thermogravimetric measurement results. Thus the composition of the structure model was in general $[Mg_{16}Al_8(OH)_{48}]A_8\cdot 24H_2O$, where A represents the guest anion. In the case of LDH–*p*-bromobenzoate intercalate we also created a $P1$ superlattice with the dimensions $12a \times 8a \times 3d_{exp}$ to obtain a better agreement with experimental data. The previous molecular modeling of a LDH-benzoate intercalate revealed the perpendicular orientation of benzoate anions with respect to the LDH layers and location of water molecules in the interlayer space [13].

Therefore a set of initial models with perpendicular orientation of the long axis of the guest anions with respect to the hydrotalcite layers and with various mutual arrangements of the benzoate rings of the anions was created. The molecules of water were situated in the space between the OH groups of the host layers and the phenyl rings of the guest anions. The charges were calculated by the Qeq method (charge equilibrium approach). The minimization was carried out in universal force field. The electrostatic energy was calculated by the Ewald summation method [14], and the van der Waals energy was expressed by Lennard–Jones potential [15]. The minimization of the total crystal energy was carried out by a modified Newton procedure according to the following strategy:

All the host layers were kept as rigid units during energy minimization, and cell parameters c, a, and β were variable. It enabled optimization of the mutual position of the host layers. All atomic positions in the interlayer space were variable as well.

The minimized models were sorted according to the similarity of the measured and the calculated diffraction pattern. After

Table 1
Formulas of the prepared intercalates and the results of elemental and TG analyses

Acid	Acid amount (g)	Formula	Found/calculated [%]		
			C	H	Weight loss
p-Methylbenzoic	0.204	$[Mg_{0.70}Al_{0.30}(OH)_2](C_7H_7CO_2)_{0.30}\cdot H_2O$	24.12/24.49	5.22/5.23	61.5/63.0
p-Bromobenzoic	0.301	$[Mg_{0.68}Al_{0.32}(OH)_2](BrC_6H_4CO_2)_{0.32}\cdot H_2O$	19.25/19.06	3.97/3.77	66.5/69.0

the minimization quench dynamics simulation was carried out in an NVT statistical ensemble (constant number of atoms, constant volume and temperature) at a temperature of 300 K. In the quench dynamics, periods of dynamic simulations are followed by a quench period in which the structure is minimized. A dynamic time step was 0.001 ps and 50,000 steps of dynamics were carried out. After quench dynamics the structures were minimized to obtain the final structure models.

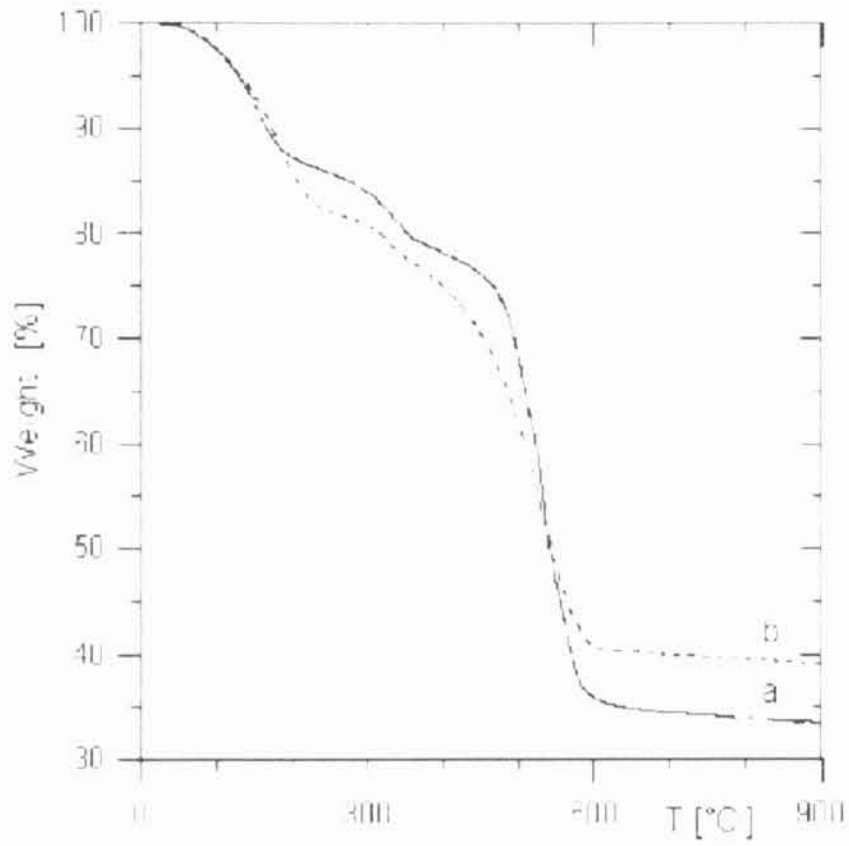

Fig. 1. Thermogravimetric curves of the *p*-bromobenzoate (a) and *p*-methylbenzoate (b) intercalates.

4. Results and discussion

4.1. Experiment

Carbonate ions are strongly held in the interlayer region of Mg–Al–CO_3 and cannot be replaced by other anions in neutral or basic medium. Also heating of Mg–Al–CO_3 in aqueous solution of corresponding carboxylic acid does not lead to intercalation in contrast to reaction with molecules containing a SO_3H group, which can be intercalated in this way [16]. Therefore single phase products were prepared using so-called memory effects, i.e., treating a calcined host powder with corresponding acid solution. The hydrothermal conditions were used to obtain products with better developed crystallites.

The composition of the intercalates prepared was determined using EDX analysis, elemental analysis, and thermogravimetry. As can be seen from Table 1, the Mg/Al ratio slightly changes during intercalation from 2/1 for the staring host to about 2.33/1 for the intercalate containing *p*-methylbenzoate anions. Probably a part of aluminum cations was dissolved during hydrothermal treatment.

Thermogravimetric curves of the intercalates are given in Fig. 1. The *p*-bromobenzoate-containing intercalate decomposes in three steps. The first step corresponds to loss of interlayer water; the observed weight loss 13% is in a good agreement with the value calculated for the intercalate containing one interlayer water molecule per formula unit (12.8%). The second weight loss is probably caused by dehydroxylation of hydrotalcite layers. The observed weight loss 8% is lower than the calculated one (12.8%) probably due to the fact that the decomposition of intercalated anions starts before the dehydroxylation is completed. The total weight loss 66.5% is lower than the cal-

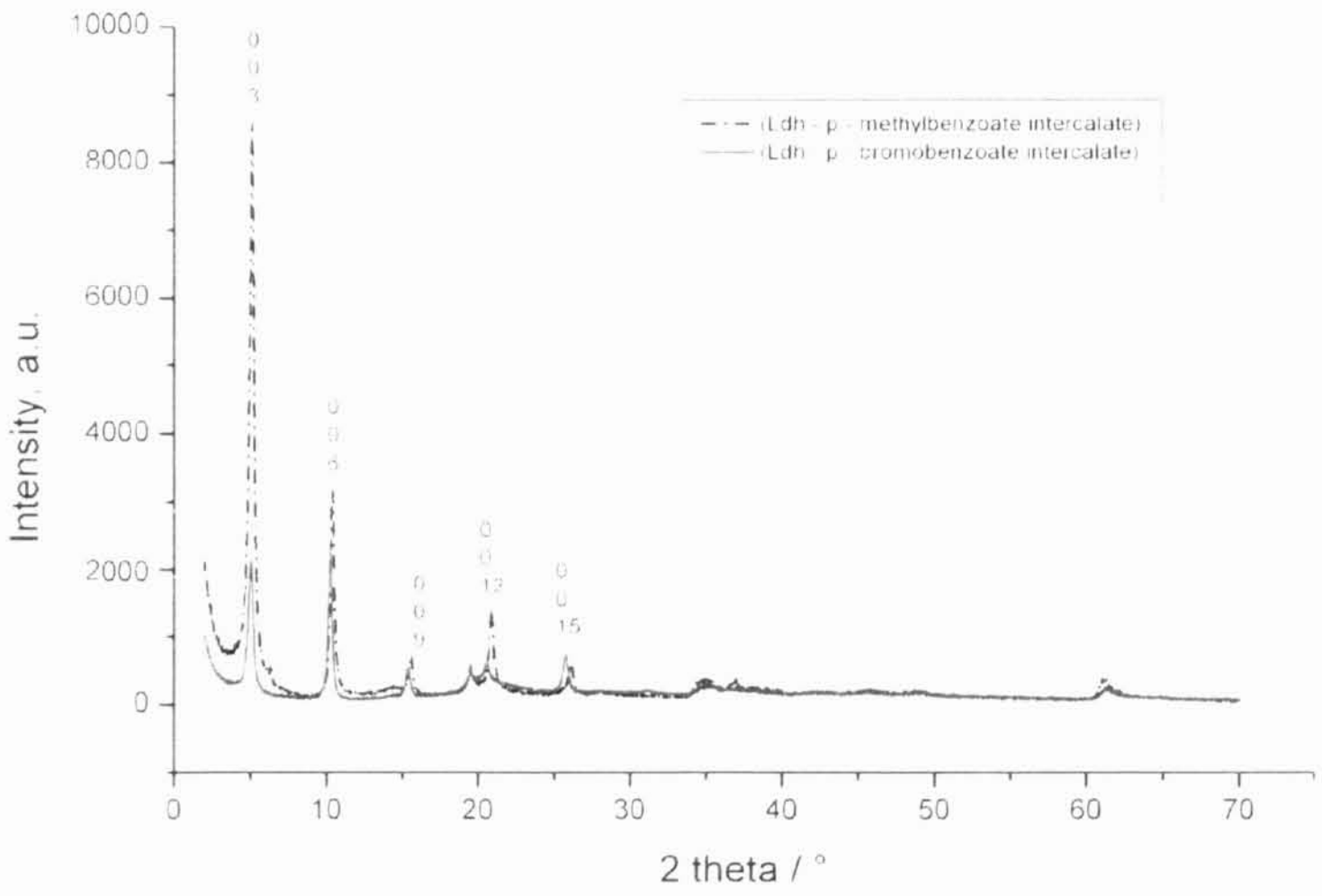

Fig. 2. Experimental X-ray diffraction pattern of LDH–*p*-methylbenzoate and LDH–*p*-bromobenzoate intercalates.

culated one (69.0%). This difference could be caused either by the fact that the oxidation of a rest of carbon is not fully completed or by the presence of a small amount of carbonate anions in the interlayer space. As the Al/Br ratio determined by EDX is 1/1, we suppose that the amount of cointercalated carbonate anions is negligible. In the case of the *p*-methylbenzoate intercalate, the interlayer water is released in the first step, but the dehydroxylation of the layers and the decomposition of the intercalated anions cannot be distinguished. The total weight loss is in a good agreement with the calculated value (see Table 1).

4.2. Molecular modeling

The experimental diffraction patterns of the intercalates with labeled basal reflexion, shown in Fig. 2, exhibit sharp basal reflections showing an order in the *c*-axis direction. The broad nonbasal reflections characterizing the LDH host framework show a certain disorder of layer stacking probably caused by turbostatic effects and by inperfect reconstruction of the hydrotalcite layers. Due to this fact the crystal structures of the intercalates exhibit a structure disorder.

The molecular modeling revealed the structure disorder of the intercalates and led to a conclusion about the mutual arrangement of the guest anions in the interlayer space. The side and the top views of the optimized structure of LDH–*p*-methylbenzoate intercalate are shown in Figs. 3a and 3b. We can see that the long axis of the guest anions in the interlayer space exhibits a departure from the perpendicular orientation about $\pm 10^{\circ}$, and in rare cases 20°. Molecular dynamics showed that guest anions are not freely distributed in the interlayer space but they tend to flock in rows with a certain disorder. Fig. 3b shows that the centers of phenyl rings are not situated in the line but they exhibit a departure of 1.5 Å at maximum from the line connecting centers of two identical phenyl rings in the neighboring cells. Calculated basal spacing $d_{calc} = 16.97$Å is in good agreement with the experimental basal spacing $d_{exp} = 16.96$ Å.

The side and the top views of the structure model of LDH–bromobenzoate intercalates are shown in Figs. 4a and 4b. While the guest anions in the interlayer space of the LDH–*p*-methylbenzoate intercalate tend to be situated in disordered rows, the structure of LDH–*p*-bromobenzoate exhibits a total disorientation of *p*-bromobenzoate anions in the interlayer space. The higher calculated basal spacing $d_{calc} = 17.40$ Å is slightly higher than experimental basal spacing $d_{exp} = 17.19$ Å that is caused by a high disorientation of guests in the structure model.

The calculated X-ray diffraction patterns are shown in Figs. 5 and 6. The higher intensity of basal reflection with respect to the others in comparison to the experimental diffraction pattern is due to the roughness of the surface of the experimental sample which is not taken into account in the calculating software. The roughness of the surface takes effect just by low values of diffraction angles and results in a decline of the intensity of basal reflection in the experimental diffraction pattern. In the case of *p*-bromobenzoate intercalate the high reflexion of bromine atoms results in higher intensity of the reflexion (0 0 6)

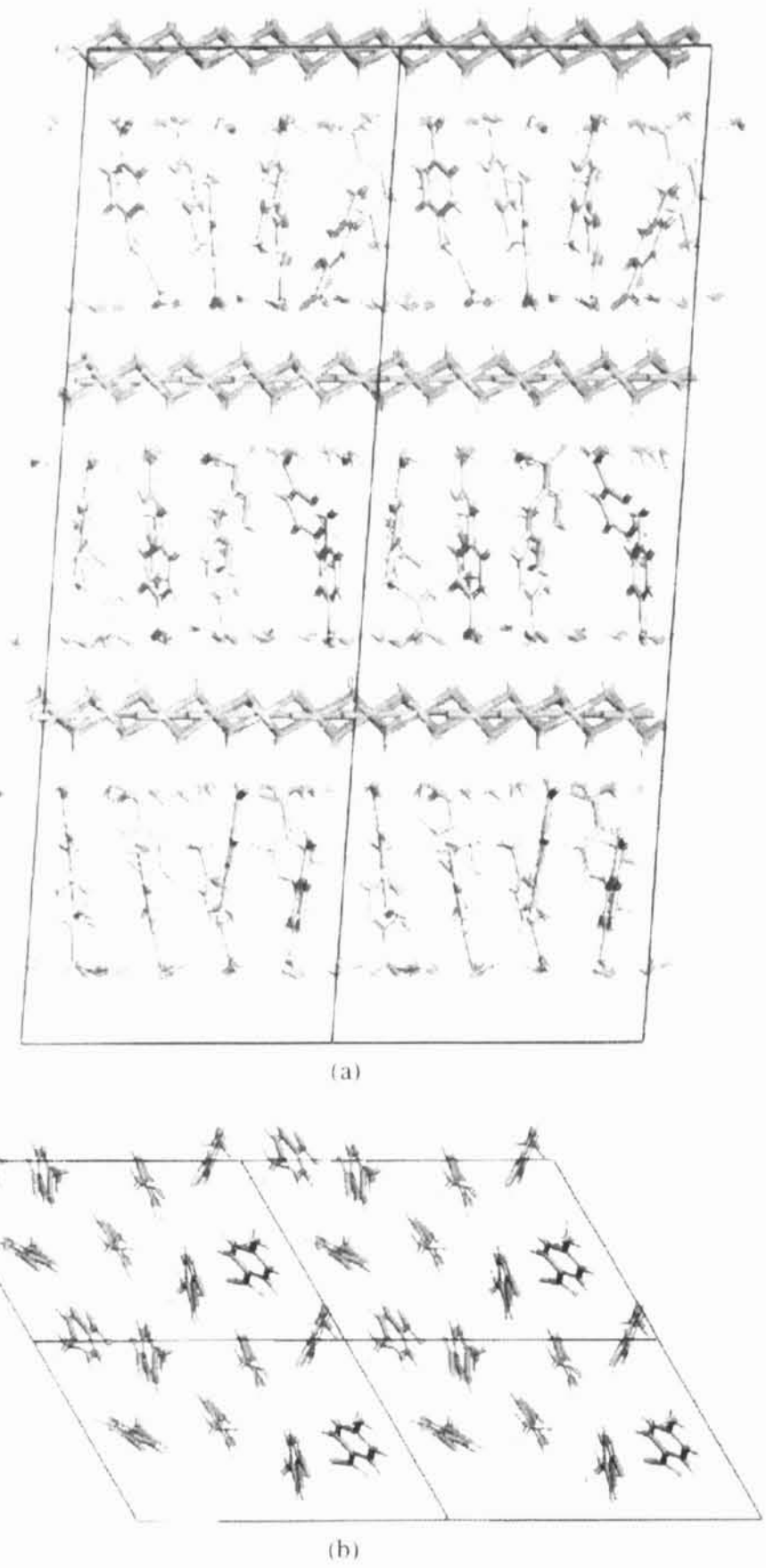

Fig. 3. (a) Side view of the optimized model of LDH–*p*-methylbenzoate intercalate. (b) Top view of mutual orientation of guests in the LDH–*p*-methylbenzoate intercalate.

in comparison to the (0 0 3) one in the *p*-methylbenzoate intercalate. We also observed that both X-ray diffraction patterns are strongly influenced by the position of the interlayer water. In the case of *p*-methylbenzoate the location of interlayer water as shown in Fig. 3a results in a higher peak (0 0 12) in comparison to the (0 0 9) one. If interlayer water is freely distributed between the benzene rings and the hydrotalcite layers it leads to growth of the peak (0 0 9) and to a disagreement of the ratio of (0 0 9) and (0 0 12) in the calculated diffraction pattern with respect to the experimental one.

In the case of *p*-bromobenzoate the intensities of (0 0 9) and (0 0 12) reflexions remain unchanged when changing location of water molecules in the interlayer space and the change of water molecules location strongly affects the intensity of reflexion

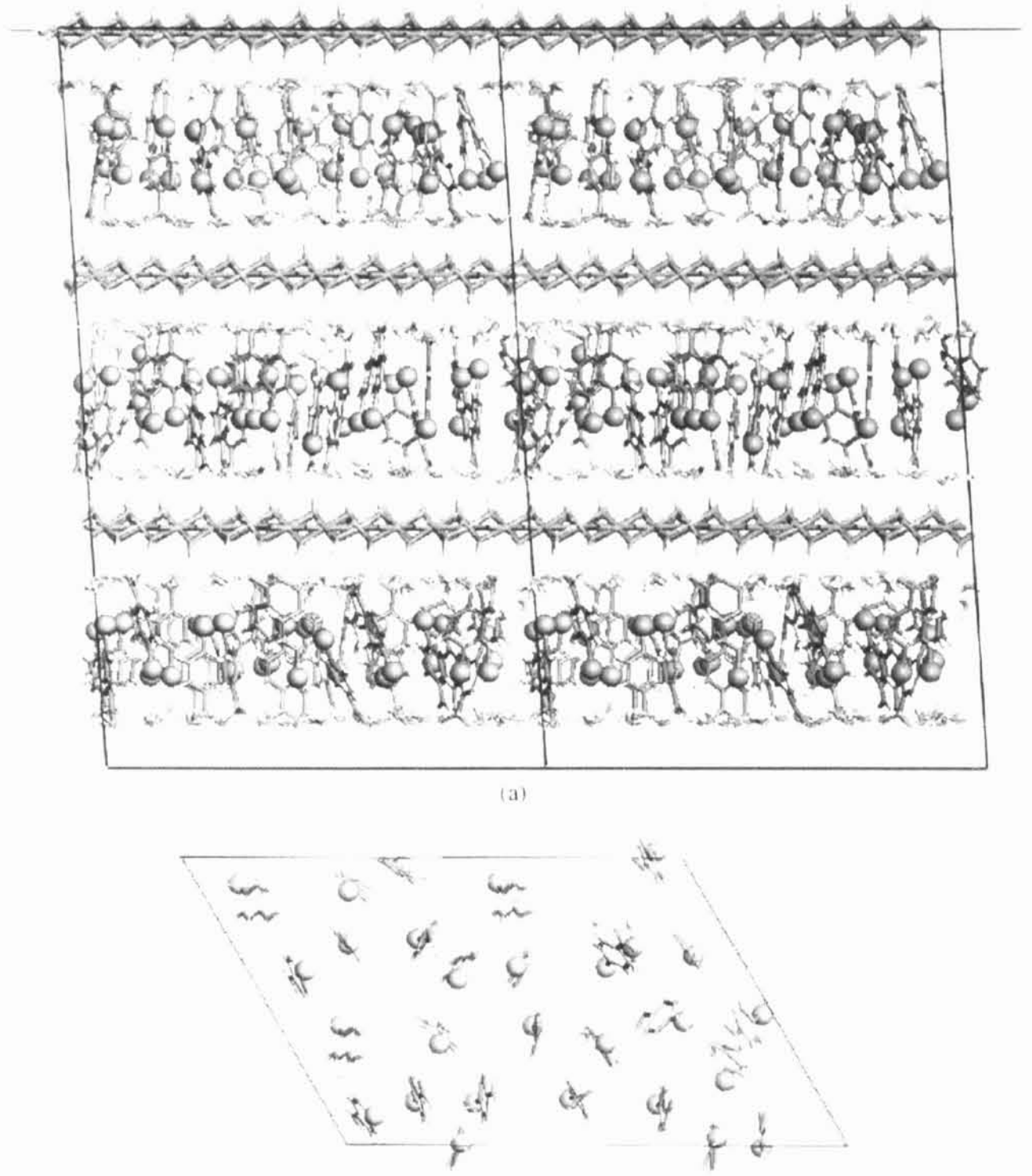

(a)

(b)

Fig. 4. (a) Side view of the optimized model of LDH–*p*-bromobenzoate intercalate. (b) Top view of mutual orientation of guests in the LDH–*p*-bromobenzoate intercalate and position of water molecules.

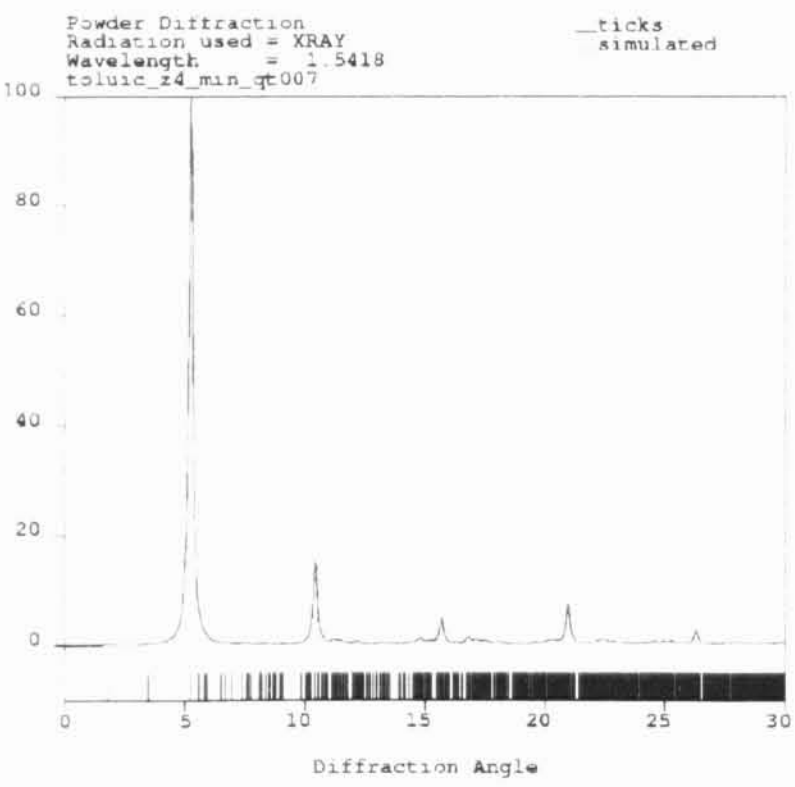

Fig. 5. Calculated X-ray diffraction pattern of LDH–*p*-methylbenzoate intercalate.

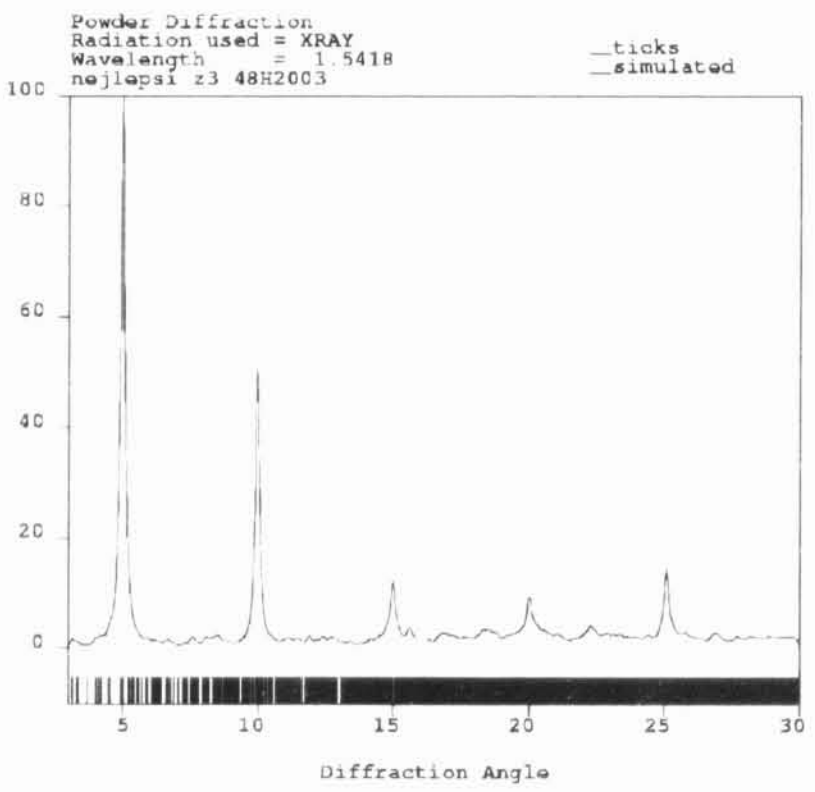

Fig. 6. Calculated X-ray diffraction pattern of LDH–*p*-bromobenzoate intercalate.

(0 0 6) only and changing their location leads to the growth of the peak (0 0 6).

These observations led to the conclusion that in both types of intercalates water molecules in the interlayer space must be concentrated in two clean-cut planes adjacent to the hydrotalcite layers coinciding with COO groups. COO groups of the guest anions are anchored to OH groups of the host layers via electrostatic interactions and hydrogen bonds. The hydrogen bonds are represented by the broken lines in the figures for illustration.

5. Conclusions

Molecular modeling enabled us to investigate the structure of the interlayer space of the LDH–*p*-methylbenzoate and LDH–*p*-bromobenzoate intercalates, i.e., the orientation of guest anions with respect to the host layers and the character of disorder of guest anions. While in the case of *p*-methylbenzoate intercalates the guests are located in rows with a certain degree of disorder, the guests in the case of *p*-bromobenzoate intercalates exhibit a total disorientation in the interlayer space. We found the role of interlayer water on the X-ray diffraction pattern profile and its clean-cut location in the interlayer space.

Acknowledgment

This work was supported by the Grant Agency of the Czech Republic, Grant 203/05/2306.

References

[1] V. Rives, Layered Double Hydroxides Present and Future, Nova Science, New York, 2001, pp. 1–48.
[2] X. Hou, R.J. Kirkpatrick, J. Inorg. Chem. 40 (2001) 6397–6404.
[3] X.Q. Hou, A.G. Kalinichev, R.J. Kirkpatrick, J. Chem. Mater 14 (5) (2002) 2078–2085.
[4] U. Costantino, M. Nocchetti, in: V. Rives (Ed.), Layered Double Hydroxides Present and Future, Nova Science, New York, 2001, pp. 435–468.
[5] M. Turco, G. Bagnasco, U. Costantino, F. Marmottini, T. Montanari, G. Ramis, G. Busca, J. Catal. 228 (2004) 43–55.
[6] A. Vaccari, Appl. Clay Sci. 14 (1999) 161–198.
[7] Y. Mitsuo, J. Ecotechnol. Res. 8 (2) (2002) 248–249.
[8] L. Latterini, M. Nocchetti, G.G. Aloisi, U. Costantino, F. Elisei, Inorg. Chim. Acta 360 (2007) 728–740.
[9] M. Ogawa, K. Kuroda, Chem. Rev. 339 (1995) 335–341.
[10] L. Lei, A. Khan, D. O'Hare, J. Solid State Chem. 178 (2005) 3648–3654.
[11] U. Costantino, F. Marmottini, M. Nocchetti, R. Vivani, Eur. J. Inorg. Chem. 10 (1998) 1439–1446.
[12] P. Comba, T.W. Hambley, Molecular Modeling of Inorganic Compounds, VCH, Weinheim, 1995, pp. 28–31.
[13] P. Kovář, M. Pospíšil, M. Nocchetti, P. Čapková, K. Melánová, J. Mol. Model. 13 (2007) 937–942.
[14] N. Karasawa, W.A. Goddard, J. Phys. Chem. 93 (1989) 7320–7327.
[15] J.E. Lennard-Jones, Proc. R. Soc. London Ser. A 109 (752) (1925) 584–597.
[16] L. Beneš, K. Melánová, V. Zima, J. Svoboda, Collect. Czech. Chem. Commun. 70 (2005) 259.